Dissertation
submitted to the
Combined Faculties for the Natural Sciences and for Mathematics
of the Ruperto-Carola University of Heidelberg, Germany
for the degree of
Doctor of Natural Sciences

presented by
Patrick Heil, M. A.
born in Fulda

Oral examination: November 30th, 2007

Shearing Cells with Single Elastic Micropillars to Influence Focal Adhesion Dynamics

Referees:
Prof. Dr. Joachim Spatz
Prof. Dr. Heinz Horner

Focal adhesions (FAs) are important adhesion sites between eukaryotic cells and the extracellular matrix: They mediate cell adhesion, spreading and motility. Over the last decade it has become evident that FAs are bi-directional mechano-chemical devices: They both exert and sense physical forces by converting biochemical signals into mechanical force and vice versa. As such, they represent a highly fascinating interface between physics and biology.

Recently, it has been shown that the intrinsic force generated by the contractile machinery of the cell that leads to FA growth can be substituted by external forces. However, the exact mechanism behind FA-mediated mechanosensing remained unclear. This unsolved question has stimulated several competing theories that attempt to model the physical principles governing the force-induced assembly of adhesion plaque proteins.

In this thesis, we present a novel, inexpensive method to micromanipulate living cells with single elastic micropillars and discuss the effect of lateral shear stress on focal adhesion dynamics of fibroblasts. We have successfully induced both growth and disassembly of FAs by shearing cells. Dynamics of single FAs and intensity profiles along their major axes have been analyzed in detail. We find distinct features for stretched respectively relaxed FAs. The presented data will be valuable for the further refinement, verification or falsification of theories in this field.

Fokale Adhäsionen sind wichtige Adhäsionsstellen zwischen eukayiotischen Zellen und der extrazellulären Matrix: Sie vermitteln die Adhäsion, Ausbreitung und Beweglichkeit der Zellen. Im letzten Jahrzehnt wurde deutlich, dass fokale Adhäsionen bidirektionale mechano-chemische Wandler sind: Sie üben nicht nur physikalische Kräfte aus, sondern detektieren diese auch, d.h. sie wandeln biochemische Signale in mechanische Kräfte um und umgekehrt. Daher stellen sie eine höchst faszinierende Schnittmenge von Physik und Biologie dar.

Kürzlich wurde gezeigt, dass die intrinsischen Kräfte, die vom kontrahierenden Zellapparat generiert werden und zum Wachstum fokaler Adhäsionen führen, durch externe Kräfte ersetzt werden können. Allerdings ist der genaue Mechanismus, der diese Reaktion fokaler Adhäsionen auf mechanische Änderungen ermöglicht, bisher unklar. Dies hat verschiedene konkurrierende Theorien hervorgerufen, die versuchen, die physikalischen Prinzipien zu modellieren, die kraft-induziertem Aufbau fokaler Adhäsionen zugrunde liegen.

In der vorliegenden Dissertation stellen wir eine neuartige Methode vor, lebende Zellen mit einzelnen elastischen Mikro-Nadeln zu manipulieren, und diskutieren dabei den Einfluss von lateralen Scherkräften auf die Dynamik fokaler Adhäsionen in Fibroblasten. Uns ist es gelungen, sowohl Auf- als auch Abbau fokaler Adhäsionen durch diese Scherkräfte zu induzieren. Die dabei entstandene Dynamik einzelner fokaler Adhäsionen und ihre Intensitätsprofile wurden eingehend analysiert. Dabei wurden grundsätzlich unterschiedliche Eigenschaften angespannter und entspannter fokaler Adhäsionen beobachtet. Die hier vorgestellten Daten können einen wertvollen Beitrag zur Verbesserung, Bestätigung oder Widerlegung von Theorien auf diesem Gebiet leisten.

Contents

Introduction and Objective

Over the last two decades, the insight has risen amongst scientists that the life cycle of cells, the building blocks of living matter, is not only determined by biochemical processes, but also by physical factors. This led to an interdisciplinary research activity where physical principles and methods are applied to biological probes. The work presented here follows this tradition, merging physical knowledge, microfabrication processes, advanced fluorescent microscopy, and biology.

One particularly interesting issue in this context was addressed in our experiments: mechanosensitivity. Mechanosensitivity describes the remarkable capability of cells to sense mechanical features of their surroundings. This is especially important for so-called *fibroblasts*, cells living in and shaping the connective tissue of animals or humans. Their main function is to maintain the structural integrity of connective tissue, and in order to do so, they constantly have to assess its mechanical features.

But how exactly are these cells able to probe the physical properties of their surroundings? How do they react to external forces or determine the stiffness of the matrix they are embedded in? And what purpose might this astonishing machinery serve for in a functioning organism?

A particularly important class of cellular mechanosensors are the so-called *focal adhesions*. At first glance, these connection sites between cytoskeleton and extracellular matrix seem to be mere anchors to the cell's surrounding. But rather than being just passive adhesion clusters, focal adhesions display intriguing features: They strengthen their grip to their substrate upon increased force applied to them. They do so by acquiring more of their constitutive proteins, thus growing in size and attaching more firmly to the substrate.

Examining the detailed nature of this mechanism and the physical principles underlying it is the subject of this thesis.

Part I

Background

1 Mechanosensitivity

1.1 The Cytoskeleton

In order to form a functional physical organism, eukaryotic cells have to perform a multitude of mechanical tasks: They have to move in space and maintain their required shape and robustness. They also have to be able to organize and rearrange their internal components as they grow, divide or adapt to altering environmental conditions. All these functions are provided by the cytoskeleton, a dynamic, three-dimensional network of protein filaments that serves as a mediator for all mechanical interactions of the cells. It consists of three primary types of fibers: actin filaments, microtubules, and intermediate filaments. Each of them has distinct mechanical properties and is constructed from smaller protein subunits that are able to self-assemble into a filamentous network (Alberts et al., 2002). Their composition and function will be described in the following section.

1.1.1 Actin Filaments

Actin filaments, also called microfilaments, are two-stranded helical protein fibers that are 5-9 nm in diameter. They are composed of subunits of the protein actin, which is the most abundant of cellular proteins. They appear crosslinked into flexible linear bundles, called stress fibers, or in networks. The highest concentration of actin is found in the actin cortex, a dense network right underneath the cell membrane.

Stress fibers are transient structures which form in response to tension and disappear when tension is released. They connect pairs of focal adhesions (see Figure 1.1). When associated with the motor protein myosin, actin stress fibers are able to exert pulling forces and are as such e.g. responsible for muscle contractions. Furthermore, actin filaments are the basis of cellular movements relative to its physical environment such as crawling, contraction, and cytokinesis. They also play an important role in linking cytoplasmic proteins through integrins and submembrane adhesion plaques to the extracellular matrix. This interaction will be discussed in detail in section 1.3 which is dedicated to focal adhesions.

1.1.2 Microtubules

Microtubules are hollow, cylindrical tubes with an outer diameter of 25 nm. They are polymers made of the protein tubulin, a heterodimer with subunits termed α-tubulin and β-tubulin. In most cells, microtubules nucleate from the so-called centrosome, which plays a key role in mitosis: It organizes the microtubules to build the mitotic spindle which pulls apart the chromosomes during cell division. Microtubules also provide a set of "roads" for organelles and vesicles to move on. There are two families of molecular motors

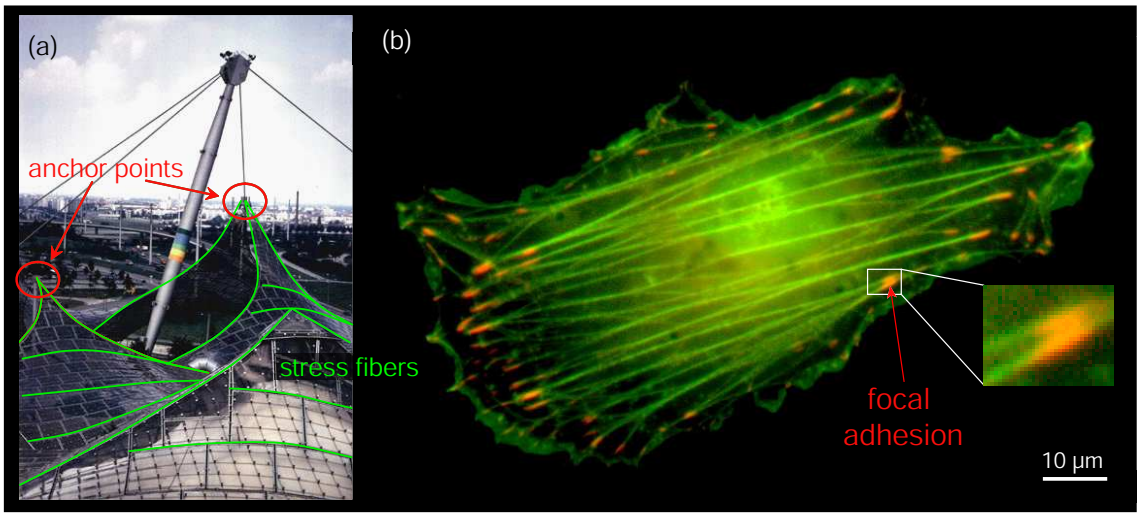

Figure 1.1: Analogy between a macroscopic building and a fibroblast in culture. Components with the same structural function are depicted in the same colors. Tension bearing stress fibers, steel cables in the case of the Munich Olympic Stadium (a) and actin fibers for the fibroblast (b), are shown in green. The counteracting anchor points, the connections to the masts of the stadium and the focal adhesions of the fibroblast, are marked in red. Note the orange color of the focal adhesions. This indicates that the actin fibers are overlapping with the actual focal adhesion markers.

that move on microtubule tracks: Kinesins which move e.g. vesicles from the centrosome to the plasma membrane and dyneins which move cargo from the cell periphery to the center (Alberts et al., 2002).

As microtubules are much more rigid than actin filaments, they act as a scaffold to determine cell shape. The interplay between these stiff structural elements and prestressed, flexible actin fibers has been proposed as the underlying mechanical principle for cell stability by the so-called tensegrity model. Tensegrity is a concept describing endoskeletal prestressed structures, i.e. structures whose boundaries have no compressed elements. It was first applied to cell mechanics by Ingber et al. who showed that linear cell stiffening upon exertion of external stress can be understood as the reaction of a tensegrity network (Ingber, 1993; Wang et al., 1993). Ingber et al. also argue that the rounding up of cells that detach from a surface or adhere to soft substrata naturally follow from their model. For a review of cellular tensegrity, see Ingber et al. (2003a; 2003b).

1.1.3 Intermediate Filaments

Intermediate filaments are about 10 nm in diameter and thus intermediate in diameter between actin filaments and microtubules - hence their name. Unlike the other constituents of the cytoskeleton, intermediate filaments can be composed of many different protein types, amongst them keratin, vimentin, desmin and nuclear lamins. Another difference to actin filaments and microtubules is that intermediate filaments have no associated motors that move on them. At the cell surface, intermediate filaments attach to specific junctions called desmosomes and hemidesmosomes. These junctions attach cells to neighboring cells or the extracellular matrix. Despite their chemical diversity, all intermediate filaments have a similarly high resistance to stretch and shear forces - higher than that

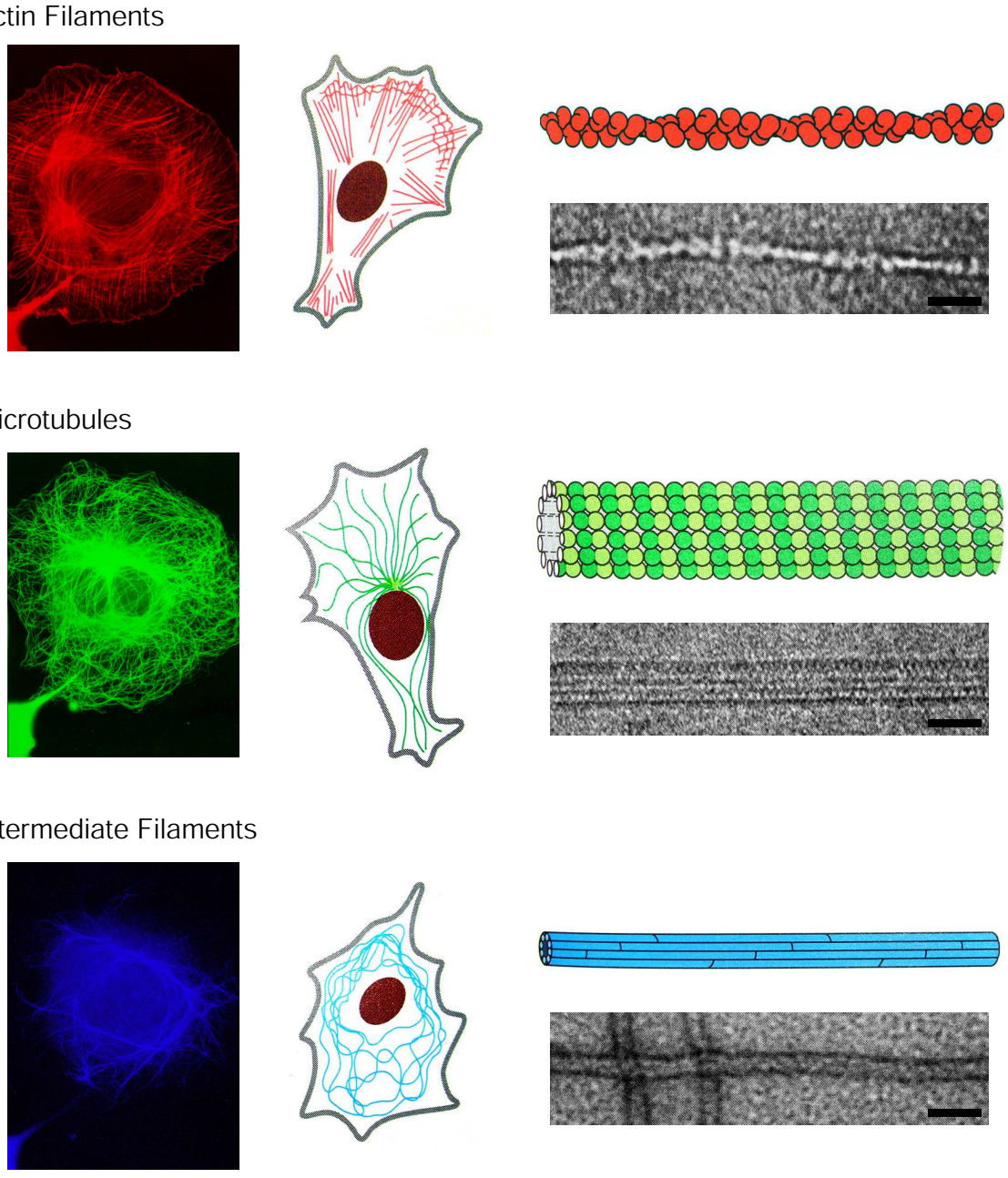

Figure 1.2: Main components of the cytoskeleton. The first column shows fluorescence images of actin filaments (red), microtubules (green) and intermediate filaments (blue) inside a cell. The second column depicts the organization of these elements with respect to the nucleus. Note the centrosome from which the microtubules radiate. The last column shows a sketch of the structure of the cytoskeletal components as well as respective electron micrographs. The scale bars are 25 nm each. Adapted from Herzog et al. (1994) and Albert et al. (2002).

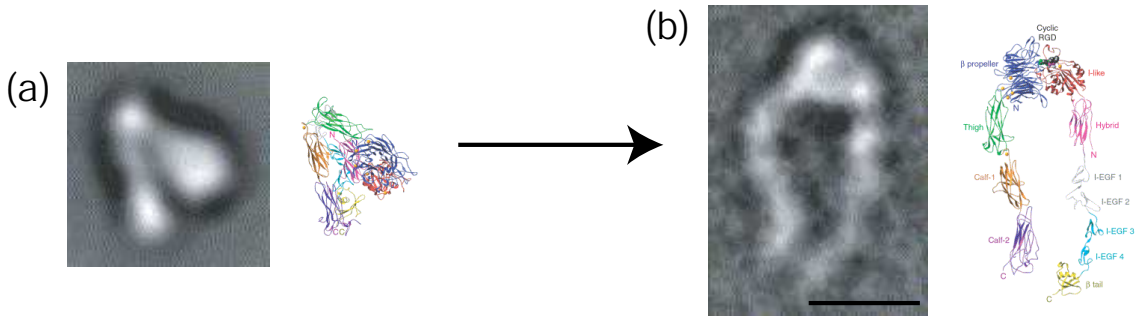

Figure 1.3: Conformational change of integrin heterodimer. Electron micrographs and corresponding atomic structures of integrins dimers in their folded (a) and activated (b) state. The scale bar is 10 nm. Adapted from Springer (2002).

of actin filaments and microtubules. Therefore, they are believed to provide a supporting framework within the cell. For example, the nucleus in epithelial cells is held within the cell by a basket-like network of intermediate filaments made of keratins (Alberts et al., 2002).

1.2 Cell Adhesion

In order to stabilize their position in an organism, cells need the ability to adhere to each other or to their surrounding tissue, the extracellular matrix. The extracellular matrix (ECM) is a complex network of secreted extracellular macromolecules that forms a supporting framework in which cells can move and adhere. Depending on the type of tissue, the amount of ECM varies: While there is e.g. hardly any matrix in epithelial tissue, connective tissue consists mainly of ECM and has only few cells in it. In most connective tissues, the ECM macromolecules are secreted by cells called fibroblasts.

Anchoring junctions at which cells connect a part of their cytoskeleton to their exterior can be divided into four groups: There are cell-cell junctions that attach intermediate filaments (*desmosomes*) or actin filaments (*adherens junctions*) to neighboring cells. These are mediated by transmembrane proteins called desmosomal cadherins respectively cadherins. Similarly, there are cell-matrix junctions that involve intermediate filaments (*hemidesmosomes*) or actin filaments (*focal adhesions*), both mediated by integrins (Alberts et al., 2002).

Integrins are heterodimeric transmembrane proteins, composed of an α and β subunit. Their extracellular part can bind to ECM proteins, for example to fibronectin via its RGD-containing domain. Importantly, integrins have shown to be mechanosensitive, i.e. they change their conformation upon application of force. When activated this way, they expose molecular binding sites that are not accessible in the non-activated state.

For adherent cells in culture, one distinguishes the *ventral side*, which is the one close to the substrate, and the *dorsal side*, which is the one not contacting the substrate.

1.3 Focal Adhesions

Of the four classes of anchoring junctions described in the above section, only focal adhesions (FAs) will be addressed in this thesis. FAs are elongated, flat structures with a length

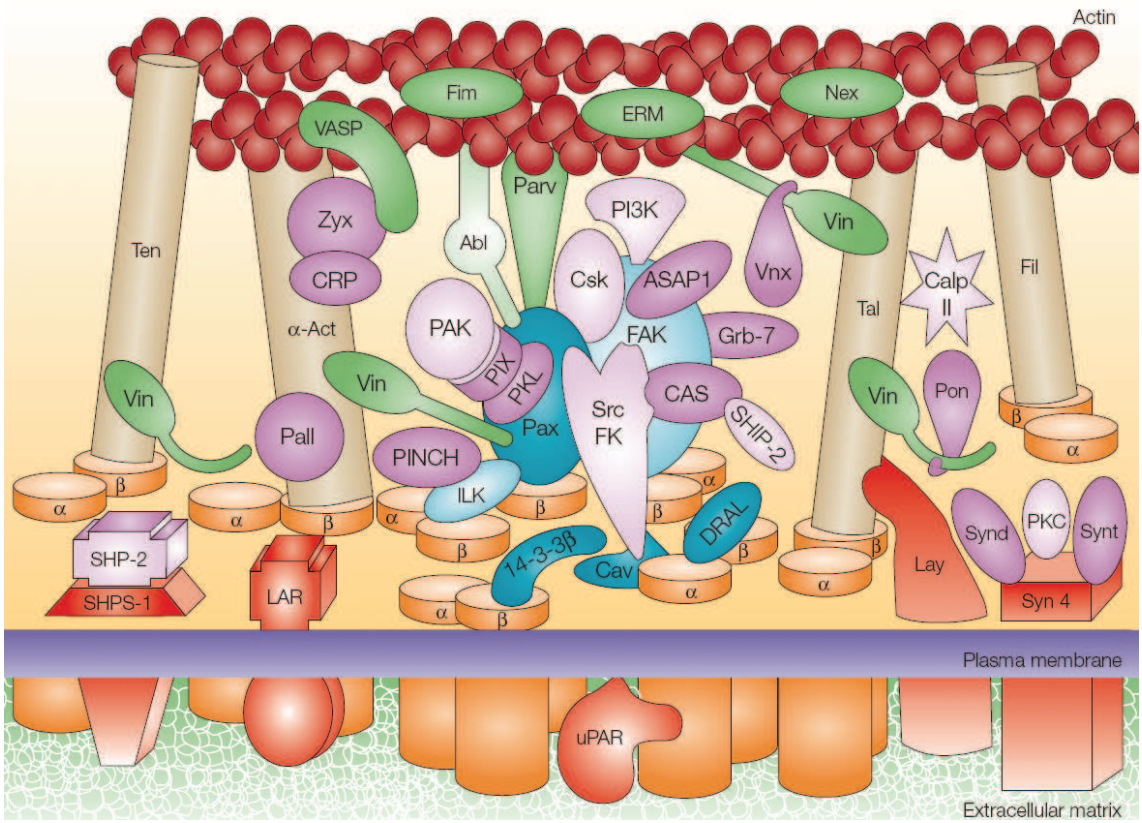

Figure 1.4: Schematic depicting the main molecular domains of cell-matrix adhesions. The transmembrane adhesion receptors, the heterodimeric (α and β) integrins are depicted as orange cylinders. Components of the focal adhesion plaque are shown between the cell membrane and the actin filaments (dark red). Amongst them are paxillin (Pax) and zyxin (Zyx), both of which have been fluorescently labeled in our experiments. Taken from Geiger et al. (2001).

of 2-5 µm, often located near the cell periphery (compare Figure 1.1). These molecular aggregates link the extracellular matrix to the actin cytoskeleton via transmembrane integrin receptors (see above) and various cytoplasmic plaque proteins. Some of these plaque proteins, like talin, α-actinin, tensin and filamin, act as a scaffold for the focal adhesion aggregate as they bind to both integrins and actin (see Figure 1.4, brown rods). Others, amongst them paxillin and focal adhesion kinase, only bind to integrins (see Figure 1.4, blue and light blue), while again others are only actin-associated (e.g. vinculin, see Figure 1.4: green) or none of all (e.g. zyxin, see Figure 1.4: purple). In total, there have been more than 50 proteins identified to contribute to focal adhesions (Zamir and Geiger, 2001). In the following, the FA end close to the cell periphery will be referred to as *back* or *rear*, while the end pointing in direction of the stress applied by the actin fibers will be called *front*.

Most FAs grow out of small actin-integrin adhesion sites called focal complexes which form at the edges of lamellopodia (Nobes and Hall, 1995; Clark et al., 1998; Rottner et al., 1999). Within less than a minute after their formation, focal complexes either perish or undergo a transformation into focal adhesions (Zaidel-Bar et al., 2003). This transformation only takes place when the adhesion site is stressed, either through cell

generated actomyosin-contractility or by an external force (Riveline et al., 2001). Hence, all FAs are prestressed by actomyosin contractility.

These highly complex structures are by no means passive anchoring points. In fact, they are dynamic structures whose assembly and disassembly mediates cell adhesion, spreading and motility. Over the last decade it has become evident that FAs are bidirectional mechano-chemical interfaces (Geiger and Bershadsky, 2001; Bershadsky et al., 2003; Wehrle-Haller and Imhof, 2002; Ingber, 2003a; Vogel and Sheetz, 2006): They both exert (Galbraith and Sheetz, 1997; Balaban et al., 2001; Beningo et al., 2001; Munevar et al., 2001; Tan et al., 2003) and sense (Riveline et al., 2001; Wang et al., 2001; Choquet et al., 1997; Davies et al., 1994; Delano-Ayari et al., 2004) forces, i.e. they convert biochemical signals into mechanical force and vice versa. This way, cells can both manipulate and explore their surrounding tissue.

Focal adhesions are identified as mechanosensors because they adapt their size to the applied tension. In most cases, FAs are elongated in the direction of the applied force. Analyzing the deformation of flexible substrates, it was found that the area of FAs is proportional to the force exerted through them with force constants around 5 $nN/\mu m^2$ (Balaban et al., 2001; Tan et al., 2003).

This also implies that cells can probe the stiffness of their surroundings. When anchored to a soft substrate, they are not able to build up high tension, and their focal adhesions will hence stay smaller than on stiff substrates (Pelham and Wang, 1997). This ability of cells to recognize the mechanical nature of substrata enables them to move in the direction of higher substrate rigidity - a phenomenon called durotaxis (Lo et al., 2000).

However, cells do not distinguish which source the force applied to a FA stems from: Riveline et al. showed that the intrinsic force generated by the contractile machinery of the cell which normally leads to FA growth can be substituted by external forces (Riveline et al., 2001).

Despite all this detailed knowledge, the exact mechanism behind FA-mediated mechanosensitivity remains unclear. This unsolved question recently stimulated several competing theories that attempt to model the physical principles governing the force-induced assembly of adhesion plaque proteins (Shemesh et al., 2005; Besser and Safran, 2006; Nicolas et al., 2004; Nicolas and Safran, 2006; Aroush and Wagner, 2006). These will be described in the following.

1.4 Physical Models

The physical mechanism of force induced FA remodeling remains unclear to date. In the past, stretch-activated ion channels were used as an explanation of the modification of FAs by external stress. Experiments have shown, however, that FAs grow or shrink in a localized manner (Riveline et al., 2001) and that the direction of the growth is oriented in the direction of the applied force. If an influx of ions caused FA remodeling, the growth would be isotropic.

Currently, there are three types of models that attempt to explain the physical mechanism of FA mechanosensitivity.

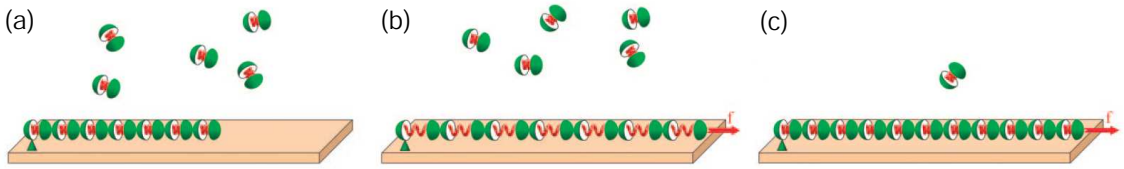

Figure 1.5: Model for FA mechanosensitivity after Shemesh et al. This model depicts the FA as a string of stretchable proteins surrounded by freely diffusion proteins (a). When this chain is stretched (b), molecules diffuse into the aggregate in order to minimize stress (c). Adapted from Shemesh et al. (2005).

1.4.1 Thermodynamic Model

The first theory by Shemesh et al. models the focal adhesion as a one-dimensional protein aggregate anchored to the substrate and subjected to pulling forces (Shemesh et al., 2005). The force is applied along the FA at discrete points with density ϕ_f. At each of these points, a force f is applied. The anchors to the underlying substrate are distributed with a density of ϕ_A. For simplicity, the FA is assumed to be composed of one type of molecule behaving like linear springs of rest length l_0.

The driving force behind FA growth upon force application is assumed to be self-assembly due to the thermodynamic principle that every system strives for a state of lowest free energy. The influx of molecules into the stretched FA aggregate (see Figure 1.5) causes a decrease of entropy and thus an increase in free energy. But this rise is smaller than the decrease of free energy due to the relaxation of the aggregate which lowers its elastic energy (and the pulling energy). Thus, this process is thermodynamically favorable and will happen until the pulling force is too small. Based on these assumptions, Shemesh et al. calculate the difference in the chemical potentials inside an outside the FA, $\Delta\mu$, depending on the distance x from the rear of the adhesion cluster as

$$\Delta\mu(x) = -(f \cdot l_0) \cdot \left[1 - \frac{\Delta\mu_0}{f \cdot l_0} + \frac{\phi_f - \phi_A}{1 + \phi_A L} \cdot (L - x)\right], \tag{1.1}$$

with L being the length of the aggregate, and μ_0 the difference in the chemical potentials of the FA molecules in the absence of pulling forces. Hence, the local influx of adhesion molecules, which is proportional to $\Delta\mu$, is predicted to vary linearly along the focal adhesion.

1.4.2 Thermodynamic Model with Mechanosensitive Elements

The second model, first developed by Nicolas et al. and later extended by Besser and Safran, describes a focal adhesion as a network of coupled springs (Nicolas et al., 2004; Nicolas and Safran, 2006; Besser and Safran, 2006). Upon stress application, both tension and compression exist in this network that can - depending on their level - lead to a conformational switch of mechanosensitive proteins. The aspect of mechanosensitive units distinguishes this model from the one presented by Shemesh et al. whose pure thermodynamic treatment does not include such features. Besser and Safran do not specify which proteins are the mechanosensitive ones - although integrins are a strong candidate: they just divide the FA in a layer of force-sensitive plaque proteins (including integrins) and

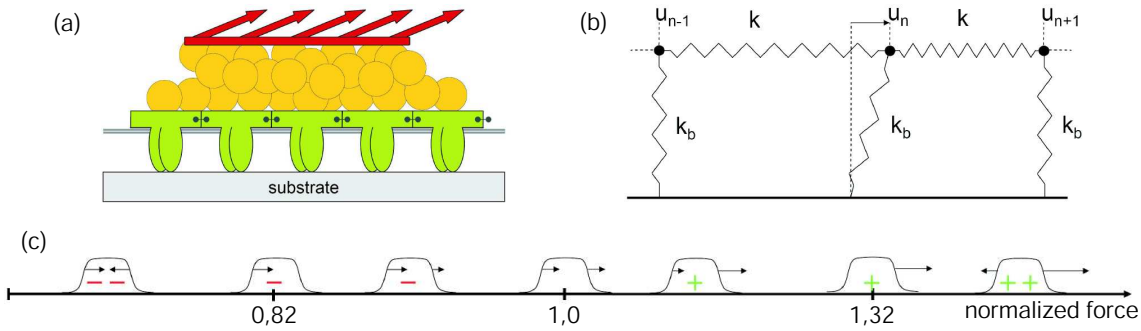

Figure 1.6: Model for FA mechanosensitivity after Besser and Safran. (a) This model divides the FA in a layer of passive plaque proteins (yellow) connected to actin stress fibers (red) and a layer of force-sensitive plaque proteins with integrins (green). The latter is described as linear chain of elastic springs anchored to the substrate (b). The model predicts different growth regimes depending on the stress applied to the focal adhesion (c). Here, the left side of the little hats depicts the back of the FAs and the right side the front. The arrows indicate the velocity of back and front, and the + and - signs mean overall growth resp. shrinking of the FA. Adapted from Besser and Safran (2006).

a layer of passive plaque proteins that connect the former to actin stress fibers (compare Figure 1.6 b). When activated, the force-sensitive plaque proteins encourage an influx of new plaque proteins, which leads to a growth of the focal adhesion. When deactivated, as it happens at the rear of the FA, plaque proteins diffuse away. To predict the velocity of the back and the front of the focal adhesions, the authors couple the elastic equation describing the lower layer and the equation describing the protein adsorption in the upper layer. From that, they derive the following partial differential equation for the concentration of the plaque protein concentration ψ:

$$\frac{\partial \psi(x,t)}{\partial t} = C_1 \left(\Delta\mu_0(\rho) - \sigma(\rho)\frac{\rho \partial \psi}{k_b \partial x} + \epsilon\psi - c\psi^3 + B\frac{\partial^2 \psi}{\partial x^2} \right), \tag{1.2}$$

where x is again the distance from the rear of the FA, k_b is the stiffness of the springs grafting the FA to the substrate (compare Figure 1.6 a) and $\Delta\mu_0(\rho)$ is the force-dependent contribution to the chemical potential that stems from the stretching of individual proteins through cytoskeletal forces. ρ is a constant that represents the average force an integrin-protein unit in the lower layer feels when it is completely connected to the actin fibers. For a more detailed interpretation of this equation, see Besser and Safran (2006).

Note the second term which is proportional to the spatial derivative of the protein concentration along the focal adhesion. This means that the protein flux is maximal at points of a high density gradient, i.e. at the back and front end of the FA.

With this knowledge and under the assumption of a constant force ρ along the FA, Besser and Safran predict certain FA growth regimes (see Figure 1.6 c). Depending on the applied stress, the amount and direction of rear and front velocities vary and determine if the FA grows or shrinks.

The confinement of the growth resp. shrinkage of the focal adhesion to its ends in the model of Besser and Safran is the clearest discrepancy to the model of Shemesh et al. who predict the plaque protein in- or efflux to be spread over the whole length of the FA.

It should be noted that both models make the assumption of a constant actin stress

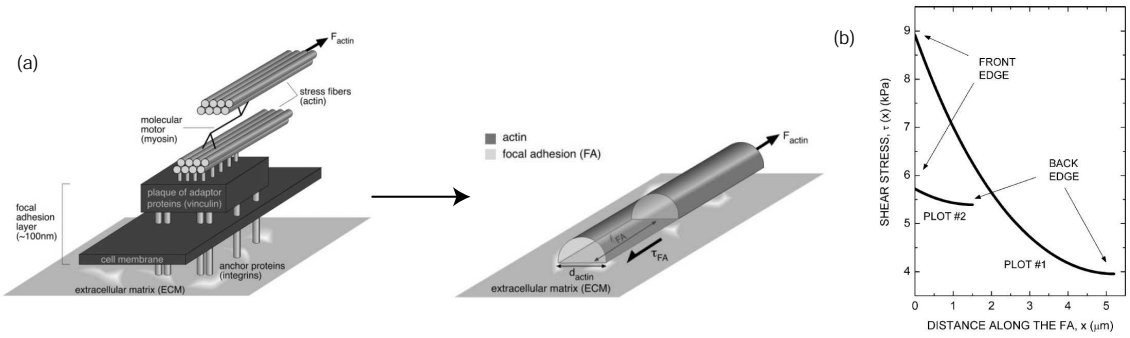

Figure 1.7: Model for shear stress distribution along a focal adhesion after Aroush and Wagner. (a) Schematic view of the FA site and of the geometry implemented in the model. (b) Predicted shear stress profile for two sets of parameters. Adapted from Aroush and Wagner (2006).

along the focal adhesion. This may not be legitimate, as was pointed out by the model presented next.

1.4.3 Composite Material Model

Finally, there is a model developed by Aroush and Wagner that describes a focal adhesion as a composite material (Aroush and Wagner, 2006). Based on this geometry, the model predicts the shear stress profile along the focal adhesion (see Figure 1.7 c) which is maximal at the front of the focal adhesion and minimal at its rear. Depending on the choice of various parameters, the curve is more or less steep. Unfortunately, this model does not (yet) include predictions about the dynamics of focal adhesions which are the focus of the work presented here.

1.5 Microstructure Assays

Traditionally, cultured cell lines are plated and observed on stiff substrates, either glass cover slips of petri dishes. This is very convenient to observe the shape and movement of the specimen, but does not allow to extract any information about the physical forces involved. To gather information about cellular forces, Harris et al. proposed a simple yet effective method to visualize traction stress: They seeded cells on thin, transparent elastomer and observed the wrinkling of this flexible substrate that was induced by the cells (see Figure 1.8 a). This yielded qualitative information about the involved forces, but to map them quantitavely from the observed wrinkles was not feasible (Harris et al., 1980).

An advancement over this technique were micropatterned flexible substrates made from polydimethylsiloxane (PDMS) that were used by Balaban et al.: They made it possible to calculate amount and origin of the forces exerted by the cells from the distortion of the microgrids (compare Figure 1.8 b). In particular, the traction force below focal adhesions was read out this way (Balaban et al., 2001). Similarly, fluorescent tracker beads have been implanted into thin polyacrylamide (PAA) gels to enable traction force microscopy (Munevar et al., 2001; Beningo et al., 2001).

Even easier access to the involved traction forces was allowed by micropillar substrates that were introduced by Tan et al.: In their experiments, cells adhered to the top of flexible

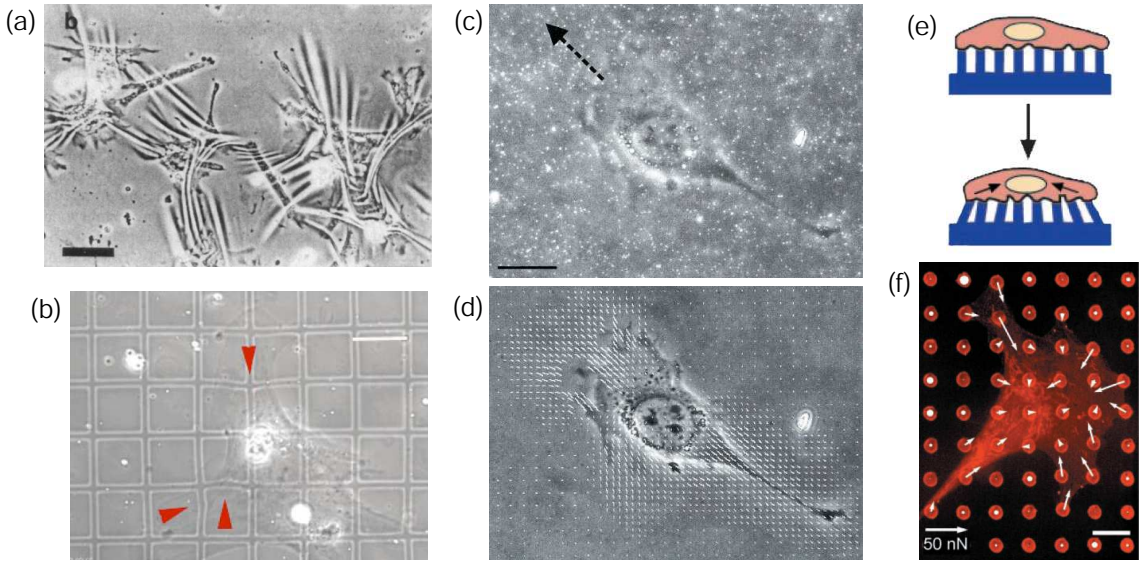

Figure 1.8: Different microstructure assays. (a) Silicone rubber substratum wrinkled by the contractility of a chicken heart fibroblast (bar is 50 µm). (b) Phase-contrast image of a rat cardiac fibroblast deforming a microstructured elastomer. The arrowheads denote distortions in the pattern, the scale bar is 30 µm. (c) Fluorescent microspheres embedded in polyacrylamide substrate, allowing the detection of the forces exerted by a NIH 3T3 fibroblast. The image was recorded with simultaneous illumination for phase contrast and epi-fluorescence. Arrows indicate the direction of cell migration. (d) Deformation vectors, derived from comparing (c) to the relaxed substrate, plotted over the phase contrast image of the cell. (e) Schematic of the principle of the micropillar array: cells seeded on top of it bend the pillars as the cells contract. (f) Fluorescence micrograph with force vectors derived from micropillar deflection. The scale bar is 10 µm. Adapted from Harris et al. (1980), Balaban et al. (2001), Munevar et al. (2001) and Tan et al. (2003).

PDMS micropillars (see Figure 1.8 e,f). The applied cellular force was proportional to the bending of the pillars and thus easily determined (Tan et al., 2003).

Part II

Materials and Methods

2 Design of the study

Our study aims at providing a detailed, time-resolved insight into the force-induced growth and disassembly of FAs. To that end, we externally shear single cells with a micromanipulation device. This increases the stress transmitted through the cytoskeleton at the rear of the cells whereas in the opposing region, cytoskeletal prestress is released (compare Figure 2.1 inset). Most importantly, we intend to induce cellular responses within minutes, not hours (as in the flow experiments of Davies et al. (1994)) in order to be able to distinguish the reaction to the changed loading situation from long-term events like altered gene expression of involved proteins. To perform this experiment, we need a biocompatible tool that is able to instantaneously exert forces on the order of 100 nN in a very controlled fashion.

During the last 20 years, micromanipulation of living cells has been conducted in a multitude of ways: Standard tools are optical tweezers, magnetic tweezers, shear flow, atomic force microscopy (AFM) and micropipette aspiration (for reviews, see Bao and Suresh (2003); Vogel and Sheetz (2006)). The forces generated by most of these tools are too weak for our purpose, with the exception of micropipette aspiration which has not been used on adherent cells, and the AFM which is not very viable for exerting lateral forces and also quite costly.

Therefore, we developed a novel, inexpensive micromanipulation tool to apply lateral force to FA sites: cell-attached single micropillars. These microstructures made from Polydimethylsiloxane (PDMS) are tailored to our purposes and functionalized with fibronectin to attract cell adhesion. Once positioned on the dorsal side of cells and adhered, we move them with a micromanipulator to shear the entire cell, perturb the intracellular tension and evoke changes in FA dynamics (see Figure 2.1). The change in internal stress is fast and drastic compared to intrinsic actomyosin-contractility. Thus we are able to see very clearly where new plaque proteins, in our case YFP-labeled paxillin molecules, are inserted into FA sites.

Moreover, the micropillars can be used as force sensors to monitor the applied lateral force in real time. Hence, force-induced FA remodeling can be systematically measured and correlated with externally applied forces.

The presented data will be valuable for the further refinement, verification or falsification of theories in this field.

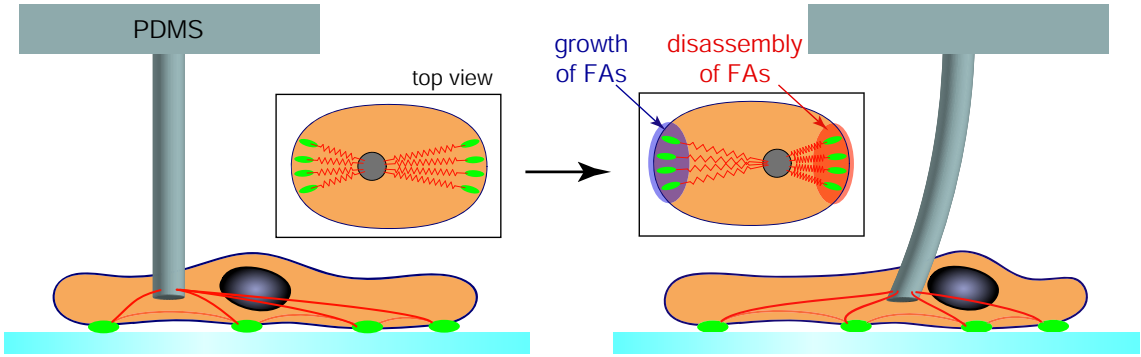

Figure 2.1: Schematic representation of the experiment. The cell is first allowed to spread for at least 30 minutes Then a microfabricated pillar coated with fibronectin is brought in contact with the dorsal side of the cell and kept there for approximately 15 minutes in order to ensure a stable adhesion between the pillar and the cell. Culture conditions are chosen such that the actin cytoskeleton (red) is in a homogeneous state (no stress fibers). When the pillar is shifted to the side, the cytoskeleton is strained and the FAs adapt their size to the new loading situation. Typically, this takes 15 minutes. In the stationary state, the sizes of the focal adhesions (green) are expected to be proportional to the forces transmitted through the cytoskeleton.

3 Experimental Techniques

3.1 Cell Culture

All experiments were performed on REF-52 cells (Rat Embryonic Fibroblasts; gift from B. Geiger, Weizmann Institute of Science, Rehovot, Israel), a cell line known to be very robust and exhibit very prominent focal adhesions. REF-52 cells stably transfected with YFP paxillin were cultured in DMEM (Dulbeccos Modified Eagle Medium, Invitrogen, Germany) supplemented with 10% fetal bovine serum (Invitrogen) and 1% L-glutamine (Invitrogen) at 37°C in a humidified, 10% CO_2 environment. All measurements were performed in an incubator that was mounted on an inverted microscope maintained at 37°C and 5% CO_2. Prior to measurements, REF cells were seeded into 60 mm glass bottom petri dishes filled with F-12 + Glutamax medium (Invitrogen, Germany) supplemented with 2% fetal bovine serum (FBS) and 1% Penicillin-Streptomycin solution (Invitrogen). This medium was chosen as it has minimal autofluorescence and thus reduces unwanted background in fluorescence images. Cells were allowed to spread for at least 30 minutes so that they were able to establish small focal adhesion clusters before experiments began. The glass bottom was not functionalized in order to slow down cell spreading and adhesion and thus enhance the affinity of the cells to the fibronectin-coated micropillars that were to be placed on their dorsal side. Both the untreated glass substrata and the small amount of FBS in the medium ensured the presence of focal adhesions that were small enough to grow yet big enough to shrink as long as experiments were conducted within 4 hours after seeding.

3.1.1 Transfection

In order to elucidate the role and state of the actin cytoskeleton in our shear experiments, we transiently co-transfected fibroblasts with fluorescent actin and zyxin for some experiments. Therefore, REF-52 wildtype cells were plated to 80% confluency in 6-well-plates. Per well, 1 µg of CFP-actin and 1 µg YPF-zyxin (both provided by B. Geiger, Weizmann Institute) were diluted in 125 µl Opti-MEM I Reduced Serum Medium (Invitrogen), gently mixed, and combined with 5 µl Lipofectamine (Invitrogen) which had also been diluted in 125 µl Opti-MEM I Medium previously. After an incubation period of 30 minutes at room temperature, 750 µl Opti-MEM I Medium were added, and the solution was gently mixed. Then, the growth medium was removed from the cells and replaced with 1 ml DMEM without serum per well. 1 ml of the diluted DNA complexes was added to each well. After an incubation period of 3 hours at 37°C in a 10% CO_2 environment, the serum-free transfection medium was replaced with serum-containing DMEM. The cells were used for experiments between 20 and 48 hours later. With zyxin being a protein present in focal

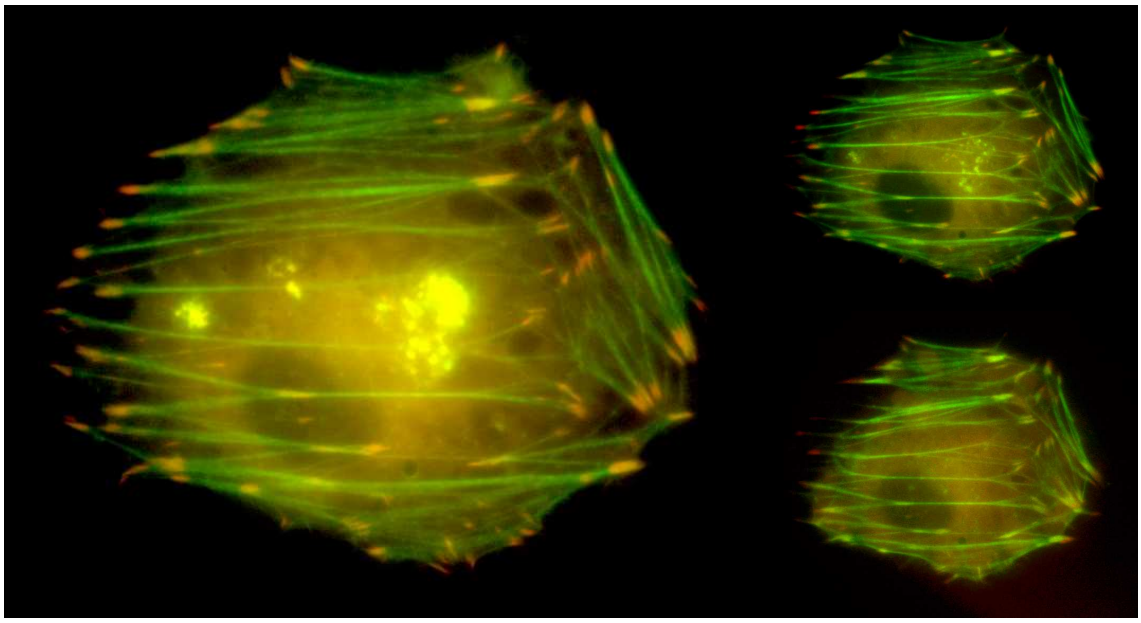

Figure 3.1: Image sequence of REF-52 fibroblast co-transfected with CFP-actin (green) and YPF-zyxin (red) 22 hours after seeding into glass bottom petri dish. The cell was subjected to an external shear force pulling to the right. Images are taken 5 minutes apart in time. Stress fibers that connect pairs of FAs can be seen as well as their rupturing due to the external shear. The unspecific fluorescence in the cytoplasm is due to an overexpression of the transfected proteins.

adhesions (see Figure 1.4, this co-transfection allowed us to monitor simultaneously the state of the actin cytoskeleton and the FA distribution of fibroblasts over extended periods of time (see Figure 3.1).

3.2 PDMS micropillars

Over the last decade, the production and use of flexible microstructures from Polydimethylsiloxane (PDMS) has become a well-established technique. Dense arrays of PDMS pillars are usually used as adhesive substrates to measure the traction forces of cells plated on top op them (Tan et al., 2003; du Roure et al., 2005). We modified this system to our needs: The arrays we used were less dense such that there would at most be one pillar per cell, and we approached the micropillars from above to the dorsal side of the fibroblasts. The following section describes the production and handling of these pillar arrays.

3.2.1 Fabrication and Mounting

Prepolymer of PDMS (Sylgard 184, Dow-Corning) was poured over an array of holes in SU-8 (Microchem, Newton, MA) made on silicon wafers via standard photolithography (Tan et al., 2003; du Roure et al., 2005; Roos et al., 2005) and cured at 65°C overnight. The dimensions of the SU-8 mask were chosen such that arrays of elastic PDMS micropillars of 5 µm diameter, a height of 11 µm, and a distance of 50 µm were received. During the process of molding, they were attached to thin glass plates (0.14 mm × 1 mm × 20 mm) via a sandwich assembly (see Figure 3.2 a). These glass plates were then used to mount the

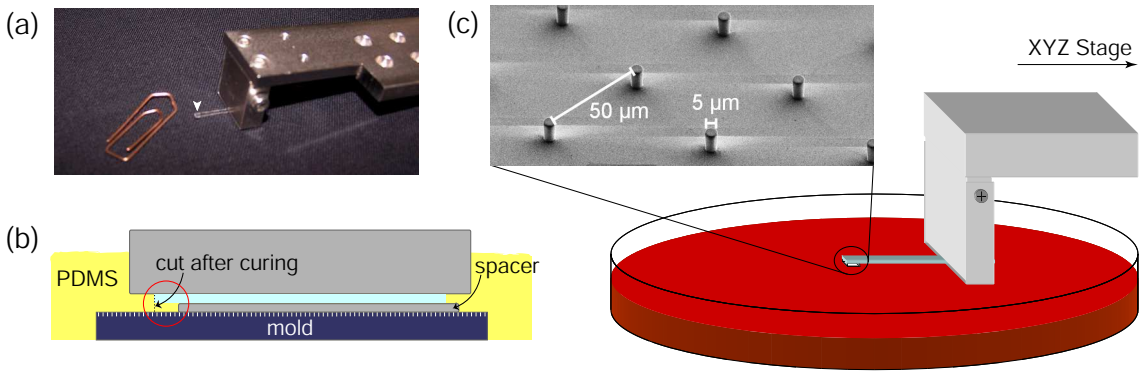

Figure 3.2: Micropillar production and micromanipulation setup. (b) A glass plate (blue) is positioned between two aluminum pieces (gray) such that there is a gap between its front and the master mold (dark blue). That gap is then filled with PDMS which is cured overnight at 65°C and cut out afterwards. The result is a PDMS pillow with micropillars that is attached to the glass plate and can easily be mounted to the XYZ-stage at the microscope (c). The inset shows an electron micrograph of a PDMS pillar array, and (a) shows a photograph of a 1 mm by 1 mm PDMS pillar array (arrow) mounted via a glass plate.

pillars to a micromanipulator (compare Figure 3.2 b). The micromanipulator is connected to an inverted microscope and comprises three micrometer screws, one of them equipped with a piezo unit in order to allow very fine positioning in z-direction (see Figure 3.3 d). Prior to experiments, the pillar substrates were treated with Hydrogen plasma (10 sec, 0.4 mbar, 150 W in Plasma etcher (100-E) from TePla) and subsequently immersed in 20 µg/ml fibronectin (from bovine plasma, Invitrogen) for 30 minutes.

3.2.2 Calibration

For the small deflections found in our experiments, micropillars can be assumed to behave like linear springs, i.e. their deflection is directly proportional to the applied force (see Tan et al. (2003)). To determine the force constant k_{pillar}, pillars were calibrated by pressing them against AFM cantilevers of known stiffness $k_{cantilever}$ after successful experiments: An AFM cantilever (whose force constant had previously been determined through its Brownian motion) was attached to a cover slip such that it was pointing upwards with its tip pointing to the right. Using the micromanipulator, the pillar to be calibrated was approached from the top and positioned behind the cantilever such that the two would barely get into contact when the pillar array was moved laterally (see Figure 3.3). A comparison between the cantilever deflection and the reference pillar deflection yielded k_{pillar}, the force constant of the micropillar (see Figure 3.3 b,c). For our conditions, this constant was around 0.2 N/m which is in accordance with theoretical predictions (see Tan et al. (2003) and du Roure et al. (2005)) for pillars of the given geometry.

3.2.3 Functionalization

In order to prevent cells from crawling up the pillars attached to their dorsal side, it was desirable to functionalize only the top of the pillars with fibronectin. For pillar arrays with inter-pillar distances of less that 10 µm, this is usually achieved by placing a drop of protein solution on top of the array, and surface tension prevents the liquid from flowing

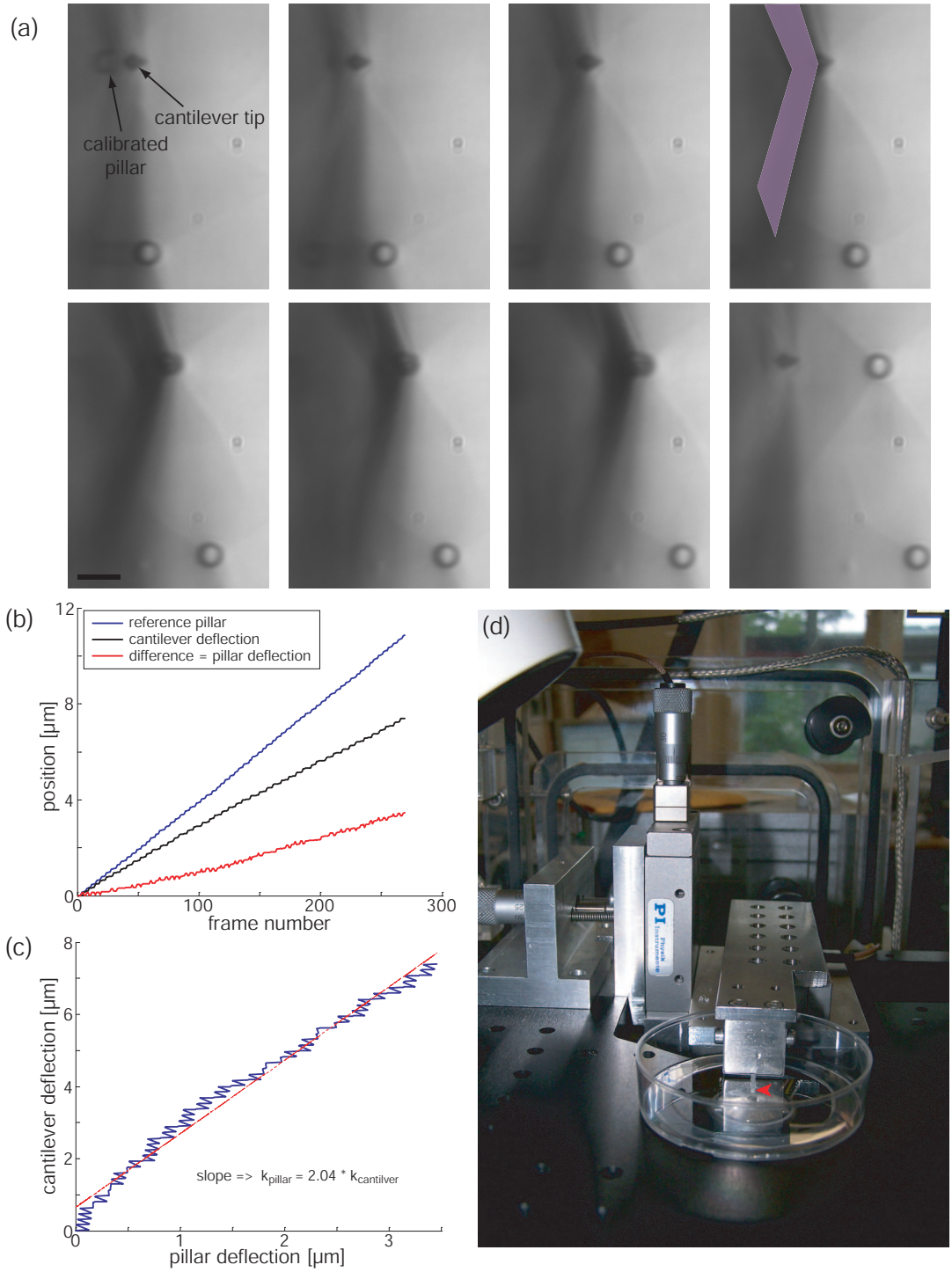

Figure 3.3: Micropillar calibration and mounting. (a) Image sequence of micropillar calibration using an AFM cantilever. The cantilever tip and the reference pillar can be seen clearly in each frame. The pillar to be calibrated, which is behind the cantilever and bending it, is only visible in the first and last frame. The upper right frame shows an outline of the cantilever. The scale bar is 10 µm. The deflection of the pillar to be calibrated is calculated from the bending of the cantilever and the position of the reference pillar (b). A comparison of cantilever and pillar deflection yield the relation between the force constants of the two (c). (d) shows a photograph of a pillar array (arrow) mounted in the micromanipulator.

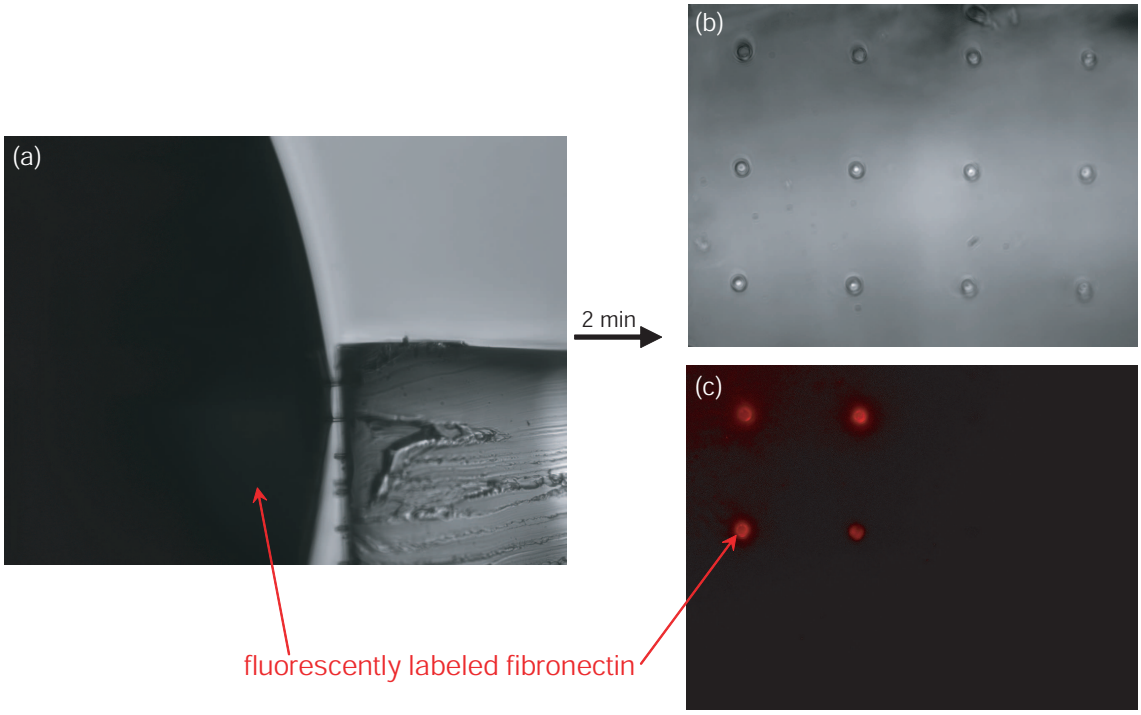

Figure 3.4: Microcontact dipping. Micropillar tips are brought into contact with a drop of fluorescently labeled fibronetin (a) and kept in this position for 2 minutes. The result can be seen in the phase contrast (b) and fluorescence (c) micrographs of the pillar array: Only the tips of only 4 pillars are coated with fibronectin. The spacing between pillars is 50 µm.

down the pillars. In our setup, this was not an option as the pillars were positioned 50 µm apart. Thus, we applied a different method: A drop of fluorescently labeled fibronectin was pressed halfway out of a tipless syringe and positioned over the microscope objective. The PDMS pillow with the pillars pointing toward the drop of liquid was brought into contact with it such that the fibronectin solution came only in contact with the tips of some pillars (compare Figure 3.4 a). These pillars stayed in contact with the solution for 2 minutes in order to induce the physisorption of the protein onto the PDMS. Fluorescence microscopy proves the success of this method (see Figure 3.4 c). Although the technique of microcontact dipping was not used in most of our experiments, it may prove useful for applications where only certain parts of a pillar array are to be functionalized.

3.3 Micromanipulation

For shear experiments, approximately round cells with focal adhesions between 1 µm and 3 µm in length were selected. The roundness selection was done in order to simplify the modeling of the stress distribution and the understanding of the shearing process. The range of FA lengths ensured that the cell was in a state where both assembly and disassembly of FAs could be induced. Using the z-piezo, a fibronectin-coated micropillar was carefully lowered onto the dorsal side of the cell halfway between its outer edge and its nucleus (compare Figure 2.1). It was left at this position for 14-18 minutes so that the cell was able to connect to it. Subsequently, the pillar was moved across the cell using

a micrometer screw. This way, the cell was sheared and the intracellular stress of the cytoskeleton was redistributed.

In Figure 7.1 we show typical phase contrast and fluorescence images for an experiment on a cell right before pulling, after pulling left and after pulling up with the microfabricated pillar. The cellular deformations caused by the pillar shift and the resulting remodeling of FA distribution can be clearly seen. Such double pull experiments were performed in order to augment the number of affected FAs and study counteracting effects of consecutive compression and stretch or vice versa.

3.4 Microscopy

Cells were observed both in phase contrast and fluorescence microscopy through an inverted microscope (Axiovert 100, Zeiss, Germany) equipped with a halogen lamp, a 100 W mercury vapor lamp (HBO 100, Osram, Germany) and an environmental chamber. Images were taken through a 63x objective (Plan-Apochromat 63x/1,4 Oil Ph3, Zeiss, Germany) and recorded with a digital charge-coupled device camera (ORCA-ER 12-AG, Hamamatsu Photonics, Germany). Typically, two frames were recorded per minute: one in phase contrast and immediately afterwards one in fluorescence mode. This process was controlled with the image acquisition software SimplePCI (Compix Imaging Systems, PA, USA).

3.4.1 Laser Auto Focus

High resolution microscopy over extended periods of time is often hindered by mechanical instabilities in the image taking system. Deviations of the position of the observed specimen as small as 200 nm in z-direction can lead to a noticeable loss in resolution. Thermal flux, as it is inevitable in a heated incubator around a microscope, worsens these fluctuations and hinders high quality time-lapse microscopy.

An approach often used to counteract this problem is manual refocusing: At least every five minutes the z-position of the objective is readjusted by taking several pictures at different heights and picking the best position. This leads to considerable photobleaching and displeased experimentators. Our solution to this problem is an automated refocusing system based on laser reflection underneath the specimen. Its mode of operation is described in the following.

For a schematic of the laser auto focus system see Figure 3.5 and for a photograph of the setup with the microscope see Figure 3.7. A laser diode (LPS-675-FC, Thorlabs, Karlsfeld, Germany) that is triggered via the digital output of a multifunction data acquisition device (NI PCI-6221, National Instruments, Austin, TX, USA) emits a 675 nm laser beam that is collimated (FC Collimation Package, F260FC-B, Thorlabs) and deflected onto a 45° red reflector (customized red reflector: same as FM02 but 0.5 inch diameter, Thorlabs). The red reflector is mounted directly under the objective revolver at an angle of 45° regarding both the incoming laser beam and the z-axis of the objective. It transmits 90% of the light below 580 nm and reflects 99% of the light above 610 nm (for a transmission curve, refer to the inset of Figure 3.7). Thus, the laser beam is coupled into the objective and focused in the objective plane. Some of the laser light is reflected back, diverted by a 50/50 beam splitter cube (BS017, Thorlabs) and detected by an amplified photo diode (PDA55-EC, Thorlabs) which is protected against stray light by two iris diaphragms connected by a cylindrical envelope. The amount of reflected light depends on the z-position of the

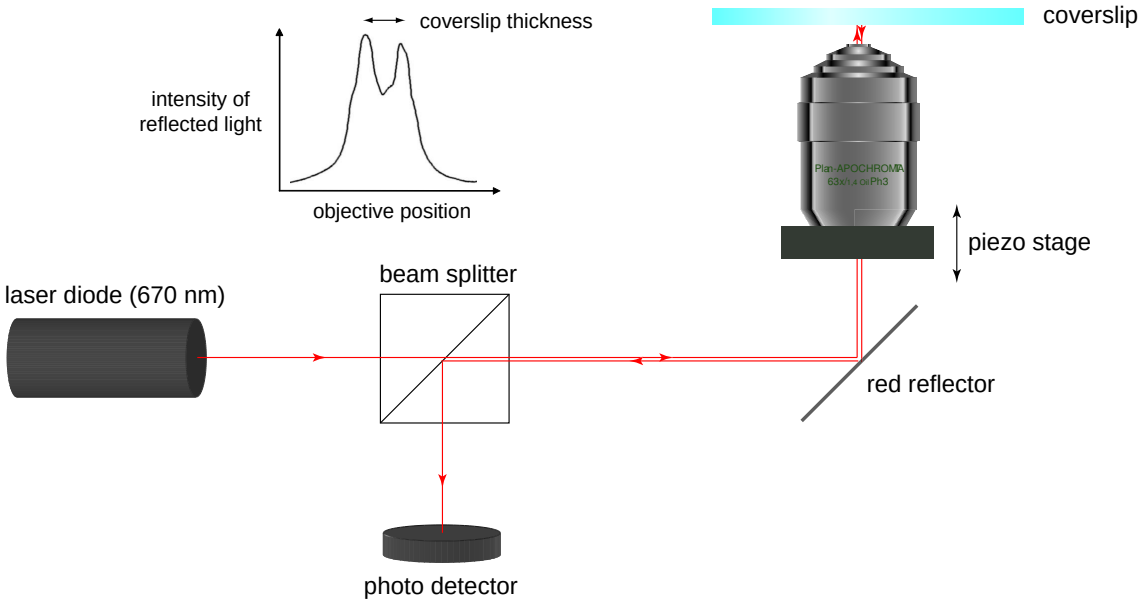

Figure 3.5: Setup of Laser Auto Focus. A beam emitted by a laser diode is coupled into the microscope objective and reflected at the coverslip. The reflected beam is deflected by a beam splitter onto a photo diode. The inset shows a characteristic photo voltage curve: The intensity of the reflected beam is highest when the objective focuses on a cover slip surface.

focal plane and is highest when it lies at either surface of the cover slip (compare inset of Figure 3.5).

The objective is mounted on a piezo z-drive (PIFOC, Physik Instrumente (PI), Karlsruhe, Germany) which is controlled through a custom program written in LabVIEW (National Instruments). This program drives the PIFOC to scan around the upper coverslip surface and reads out the voltage of the photo detector for each z-position (compare Figure 3.6 b). A parabola is fitted to the resulting curve, and the PIFOC moves the objective to a predefined offset above its maximum. Provided this offset has been defined correctly previously for the desired focal plane and the distance between this focal plane and the upper surface of the coverslip does not change, a picture can be taken now that it is precisely in focus.

The precision of this system can be estimated from the noise level of repeated measurements of the maximum of the fitted parabola (see Figure 3.6 c). It is around 100 nm and thus well below the resolution limit of optical microscopy. With the settings we used, it took the program 3 seconds to find the desired focal plane. As we usually only took one picture per minute, the laser auto focus could thus conveniently be integrated in the picture taking process and rendered manual refocusing unnecessary.

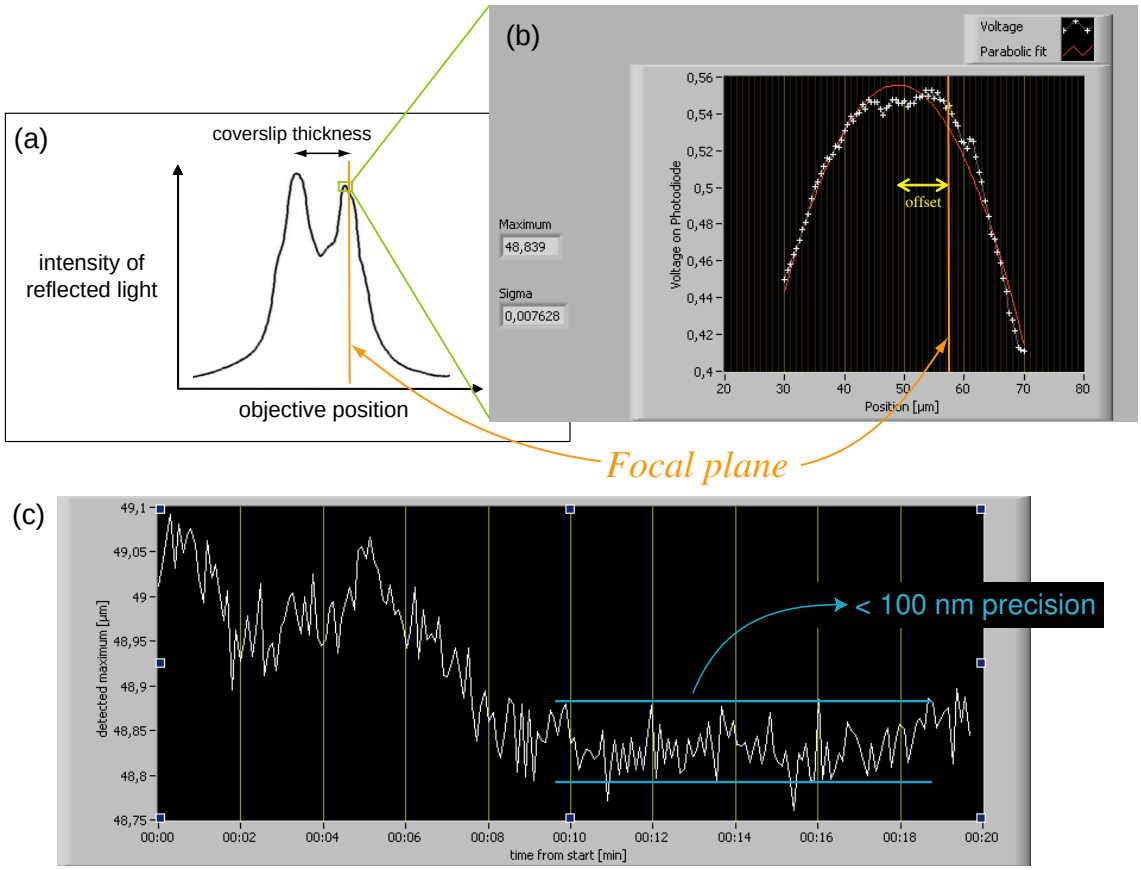

Figure 3.6: Precision of the Laser Auto Focus. The dependence of the amount of reflected light on the vertical position of the microscope objective is shown in (a). The tip of this curve is automatically scanned and fitted to a parabolic polynomial (b) by a custom LabVIEW program. Both curves show the position of the focal plane (orange) which has a constant distance to the maximum of the reflection curve of 9 µm for fluorescence pictures of FAs . Repeated determination of the fitted maximum (c) demonstrates the precision of the system which is around 100 nm and thus below the resolution limit of optical microscopy. The slow fluctuations visible in this graph are due to the mechanical instabilities that the Laser Auto Focus is to counteract.

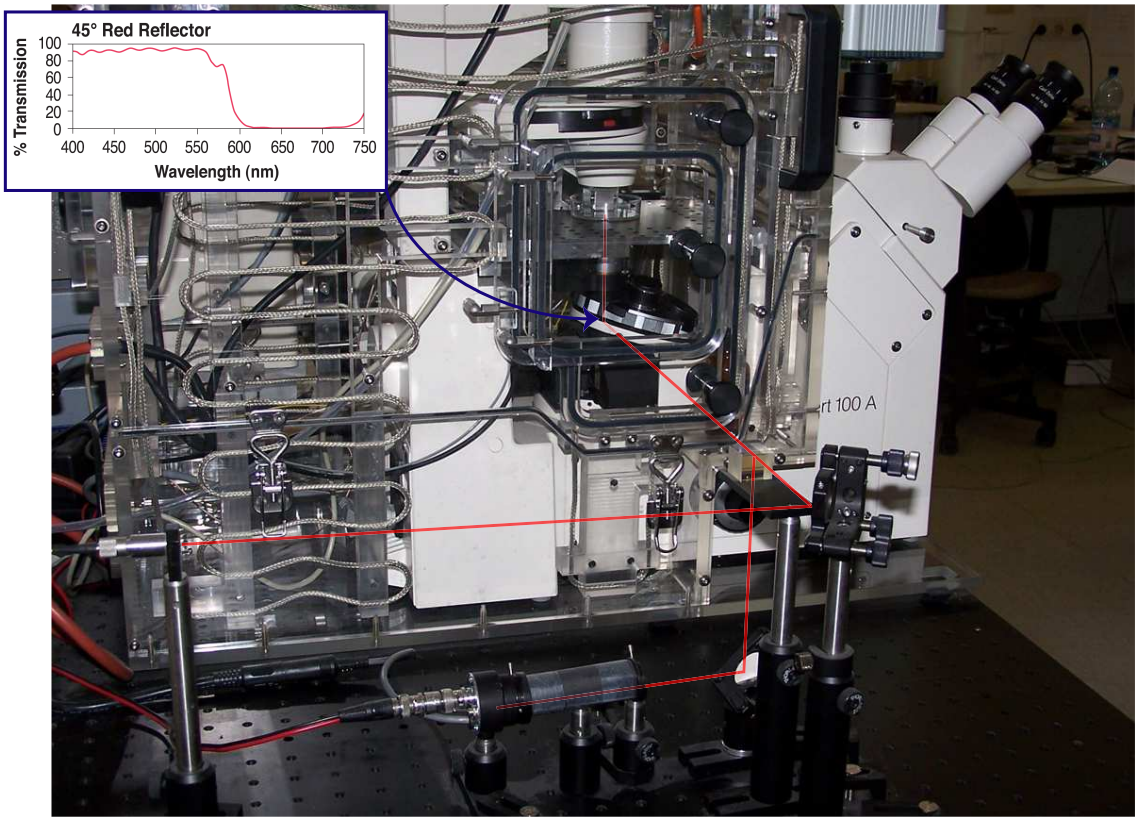

Figure 3.7: Photograph of the Axiovert 100 microscope with incubator and Laser Auto Focus. The path of the laser beam is shown in red: The beam is emitted by a laser diode (not shown), collimated by a collimator, deflected onto a red reflector underneath the objective revolver and coupled into the microscope objective. After reflection at the cover slip, it follows the same path backwards until it is diverted by a beam splitter onto an amplified photo detector diode. The detector is protected against stray light by two iris diaphragms connected by a cylindrical envelope. The incubator is made of plexiglass and heated by a heating wire. Its upper half can be taken off in order to allow easier access to the microscope when the incubator is not needed.

4 Image Processing

4.1 Fluorescence Images

Image analysis of the YFP-paxillin fluorescence was performed on stacks of uncompressed 8-bit grayscale TIFF images. Both ImageJ (version 1.37c, developed by Wayne Rasband at NIH, Bethesda, USA, http://rsb.info.nih.gov/ij/) routines and custom Matlab codes were used to process time-lapse sequences with the following steps:

4.1.1 Preprocessing

Fluorescence image sequences were preprocessed in ImageJ: First, they were registered with the plugin "StackReg" (Thvenaz et al., 1998). This algorithm performed very well in correcting the drift between subsequent images in a time-lapse sequence except for frames between which the cytoplasm - and with it the centroid of fluorescence intensity - was displaced due to micropillar movement. For these timepoints, the spatial drift was corrected manually. Subsequently, fading intensity due to photobleaching was corrected with the plugin "Bleach Correction".

4.1.2 Kymographs

Kymographs of single FAs were made by rotating the preprocessed fluorescence stacks in ImageJ such that the major axes of the FAs were horizontal, cropping them, and reslicing to switch the time axis and the y axis. Thereafter, stacks were z-projected using the Standard Deviation option, resulting in images with time located on the y axis and distance on the x axis. The kymographs were then converted to 8 bits and saved.

4.1.3 Segmentation

Threshold based segmentation and evaluation of single focal adhesion dynamics were performed by custom Matlab codes in Matlab 7.1 (The MathWorks Inc., Natick, MA, USA):

First, the image background - and with it unspecific fluorescence in the cytoplasm - was identified using a rotationally symmetric Gaussian highpass filter and removed (see Figure 4.1 a-c). Then, high frequency noise was eliminated by convolving the image with a Gaussian lowpass filter (see Figure 4.1 d). Finally, a threshold based segmentation marked all pixels above a certain intensity as FAs (see Figure 4.1 e, white).

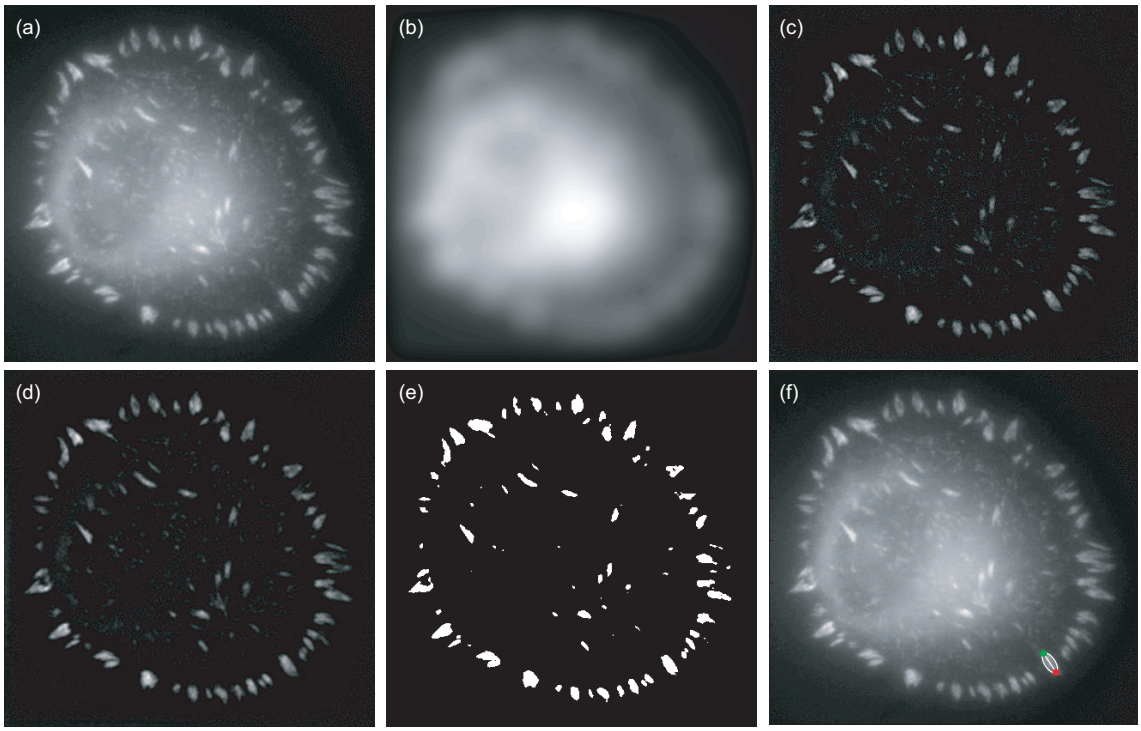

Figure 4.1: Steps of the segmentation algorithm. (a) shows the original fluorescence picture of which is convoluted with a Gaussian highpass filter (b). The difference between the two (c) eliminates background from uneven illumination and unspecific fluorescence in the cytoplasm. High frequency noise is removed with a Gaussian lowpass filter (d) before a threshold segmentation is applied (e). (f) shows an exemplary ellipse with major axis (white), front (green) and back (red) end fitted to a FA of interest.

4.1.4 Extraction of Focal Adhesion Dynamics

An ellipse was fitted to each detected FA of interest, and the ends of its major axis were defined as back and front of the FA, where front is always the part that is closer to the nucleus (see Figure 4.1 f). Before differentiating the time-dependent back and front position, these data had to be smoothed in order to prevent the resulting velocities from being overly noisy. For this, we applied the "smoothing cubic spline" function that is implemented in Matlab and determines the median between a cubic spline fit and a linear fit (see dashed lines in Figure 7.2).

4.2 Phase Contrast Images

Phase contrast images depicted the outline of the examined cell, the micropillar on its top and at neighboring, free micropillars. Micropillars display concentric Newtonian rings under phase contrast illumination. This fact was exploited by the custom algorithm described in the following.

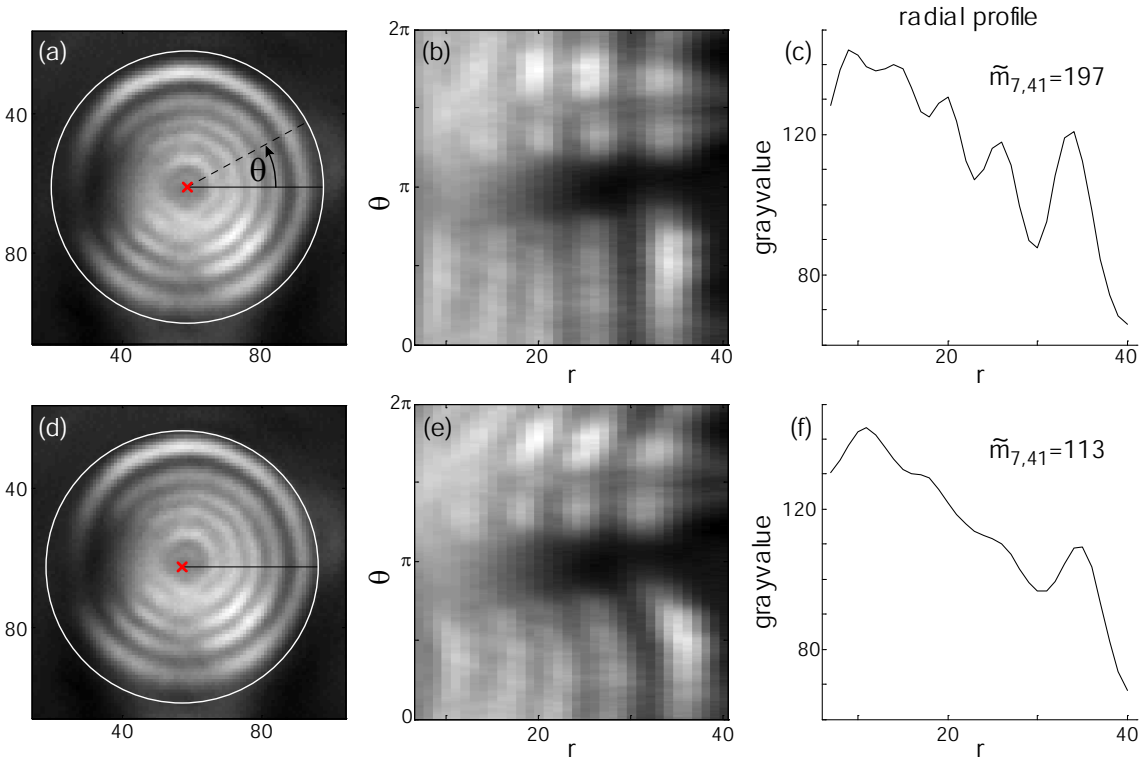

Figure 4.2: Principle of ring center detection algorithm. Images of micropillars showing interference rings (a,d) are unwrapped (i.e. transformed to polar coordinates) around the subpixel coordinates to be tested (red x). In (a), the tested coordinate is at the center of the rings, while in (d), it is shifted to the lower left. The resulting unwrapped pictures (b,e) display lines that become straighter the closer the tested position is to the center of the circles. Thus, the angle-averaged radial profile for a tested coordinate at the center of the rings (c) shows more fluctuations than the profile for an off-center coordinate (f). This is reflected in the values of the symmetry metric $\widetilde{m}$.

4.2.1 Force Detection

To evaluate the forces that were applied via the micropillar to the cells, it was necessary to find the deflection of the micropillar connected to it with subpixel resolution. Hence, we determined the time evolution of two pillars: the pillar that was connected to the cell and a free neighboring reference pillar, which was not bent. To gain the required precision, we used the fact that the micropillars appear as concentric ring structures in phase contrast images (compare Figure 7.1 d-f). Our algorithm assigns a concentricity rating to each sub-pixel coordinate in question by unwrapping the picture (i.e. transforming it to polar coordinates) around the respective position and evaluating the angle-averaged radial profile with the following symmetry metric:

$$\widetilde{m}_{r_{min},r_{max}} = \sum_{i=r_{min}}^{r_{max}} |g(r=i) - g(r=i-1)|, \tag{4.1}$$

where r_{min}, r_{max} and g are the minimal considered radius, maximal radius and average gray value at a certain radius, respectively.

Coordinates close to the center of the rings cause rather straight lines in their unwrapped

picture (compare Figure 4.2 b), which lead to big fluctuations in the angle-averaged profile (see Figure 4.2 c) – while points that are off-center cause s-shaped lines (see Figure 4.2 e) and thus a smoother radial profile (see Figure 4.2 f). The higher the fluctuations in the radial profile, the higher the value of the symmetry metric $\widetilde{m}$.

To increase performance, regions within circles were automatically detected on a down-sampled image via a circular hough transformation. Then, the position of the center of the rings was iteratively refined by employing the algorithm described above with decreasing step size. The coordinate with the highest symmetry metric $\widetilde{m}$ was assumed to be the center of the circles.

Deflection of the micropillar on top of the cell was subsequently computed as the change of distance to an adjacent pillar and multiplied with the calibrated force constant to yield the total external force applied to the cell. This vector was projected onto the major axes of FAs such that positive values mean external stress pointing from back to front of the respective FA.

The spatial resolution of this algorithm was around 20 nm for good picture quality which corresponds to 0.2 pixels or 4 nN for our system. However, uneven illumination or dirty pillars can significantly reduce this performance.

All computations for the measurement of micropillar deflection were done after experiments in the Matlab environment. It took 3 seconds to evaluate one pair of pillars with our algorithm on a standard desktop computer (Intel Pentium 4, 3 GHz, 2 GB RAM). Thus, the program could in principle be extended to monitor and control forces in real time, provided an XY-stage that can be controlled through a computer.

5 Modeling of Stress Propagation Through the Actin Cytoskeleton

The experimental method described in the previous chapters yields no information about the exact amount of stress applied to a given focal adhesion. By measuring the micropillar deflection, it can only be deduced how much external force is applied in total.

In order to shed some light on the distribution of this force to the FA assembly, simulations of stress propagation through the actin cortex were employed. This was done in collaboration with Raja Paul and Ulrich Schwarz (Bioquant, University of Heidelberg, Germany) and is presently being published (Paul et al., 2007).

5.1 Network Definition

Following earlier approaches to provide a simple model for stress propagation inside adherent cells (Stamenovi and Coughlin, 2000; Boal, 2002), the simulations were based on modeling the actin cytoskeleton as a two-dimensional network of elastic cables.

The joining points of the cables in this model are called nodes. The force acting on such a node due to the deformation of a link to length l reads

$$\vec{F} = \begin{cases} E_c A_c \, (\frac{l}{l_r} - 1) & \text{for} \quad l > l_r \\ 0 & \text{for} \quad l \leq l_r, \end{cases} \tag{5.1}$$

where E_c is the cable's Young modulus, A_c is its cross-sectional area and l_r is its resting length. As described by this formula, a cable network accounts for the observation that in cultured cells, elastic cytoskeletal elements buckle under compressive load. Before application of external force, the FAs already experience force from actomyosin-generated prestrain in the CSK. In our model, this corresponds to a resting length l_r which is smaller than the initial fiber length l_0.

For more details about the properties of the cable network, refer to Paul et al. (2007).

5.2 Fitting Experimental Data into the Model

The actin cytoskeleton was modeled as a prestressed, two-dimensional cable network connected to the substrate only at discrete anchoring points. These anchoring points were positioned such that they would match experimentally observed FA distributions of distinct cells. After extracting the adhesion point coordinates from the experimental data by image processing, they were suitably rescaled to fit into the network model. Because

the model assumes point-like adhesions, the threshold for segmentation was used in such a way that all FAs obtained are of compact shape, that is FAs with irregular shapes are split into two neighboring FAs. To make sure that the results are not affected by network symmetries, the regular spacing between the nodes was chosen to be small compared to the average distance between the adhesion points.

5.3 Simulation

After constructing the simulation system, the resting length of the cables was reduced step by step until the desired prestress was achieved in the cellular system. Once the necessary quantities of the prestressed cell were measured, a circular region at the center of the cell was selected. This mimicked the contact area of the micropillar placed on top of the cell. All nodes and cables under the circular face of the pillar were glued to it and moved along with the pillar. However, nodes and the cables which were outside the periphery of the pillar but directly connected to the nodes under the pillar could move when force was applied to them. In the simulation, the pillar was moved step by step up to 5 l_0. During the simulation, equilibrium was established by iteratively solving the equilibrium equations for all nodes until all of them were simultaneously satisfied.

Part III

Results

6 Qualitative Observations

In the course of the measurements on sheared fibroblasts, several observations have been made that do not directly affect the quantitative results on focal adhesion dynamics but shed light onto experimental circumstances. These shall be presented in the following chapter.

6.1 Actin Cytoskeleton

One question to be resolved was whether in our experiments, actin was present in the form of fibers or just as a continuous actin cortex. The first case would have implicated that the transmission of shear force to the FAs depended on the distribution of the actin fibers.

For experiments, cell medium was supplemented with only 2% FBS in order to keep the cells from fully spreading within an hour, as it would be the case for 10% FBS. Thus, we were able to work for several hours with cells with a very active metabolism because they were still in the process of spreading. These cells display FAs that are small enough to have the potential to grow, yet big enough to be able to shrink or disassemble upon lowered tension. The role of the actin cytoskeleton for cells in this intermediate state was examined using REF-52 fibroblasts co-transfected with CFP-actin and YFP-zyxin, the latter being a marker for FAs (see section 1.3). Figure 6.1 shows an image sequence of a cell 2 hours after plating - starting 14 minutes after the micropillar was lowered onto the dorsal side of the cell. Besides the effect of the pillar shift, an immediate deformation of the cell and force-induced FA growth (which will be addressed in detail in the next chapter), one can clearly see that there are no major stress fibers present. A close look at the images reveals an increased actin concentration at the periphery of the cell. This was observed in most specimens and might be interpreted as a ring of stress fibers or just a thicker actin cortex due to the proximity of the upper cell membrane in this region. In any case, our protocol guaranteed that the area between the FAs and the middle of the cell, from where micropillar-generated stress would originate, contained no actin fibers.

This knowledge justified the assumption that the distribution of stress among FAs varies smoothly and is not concentrated to certain FAs that might be connected to the micropillar via actin stress fibers. Furthermore, it justified modeling the actin cytoskeleton of the sheared cells as a uniform cable network as presented by Paul et al. (2007) and described in chapter 5.

As it was found that for our experimental conditions the actin cytoskeleton was in a state where there were no stress fibers formed yet, we refrained from co-transfecting cells with fluorescent actin and a FA marker in most experiments and used the REF-52 cell line stably transfected with YFP-paxillin instead.

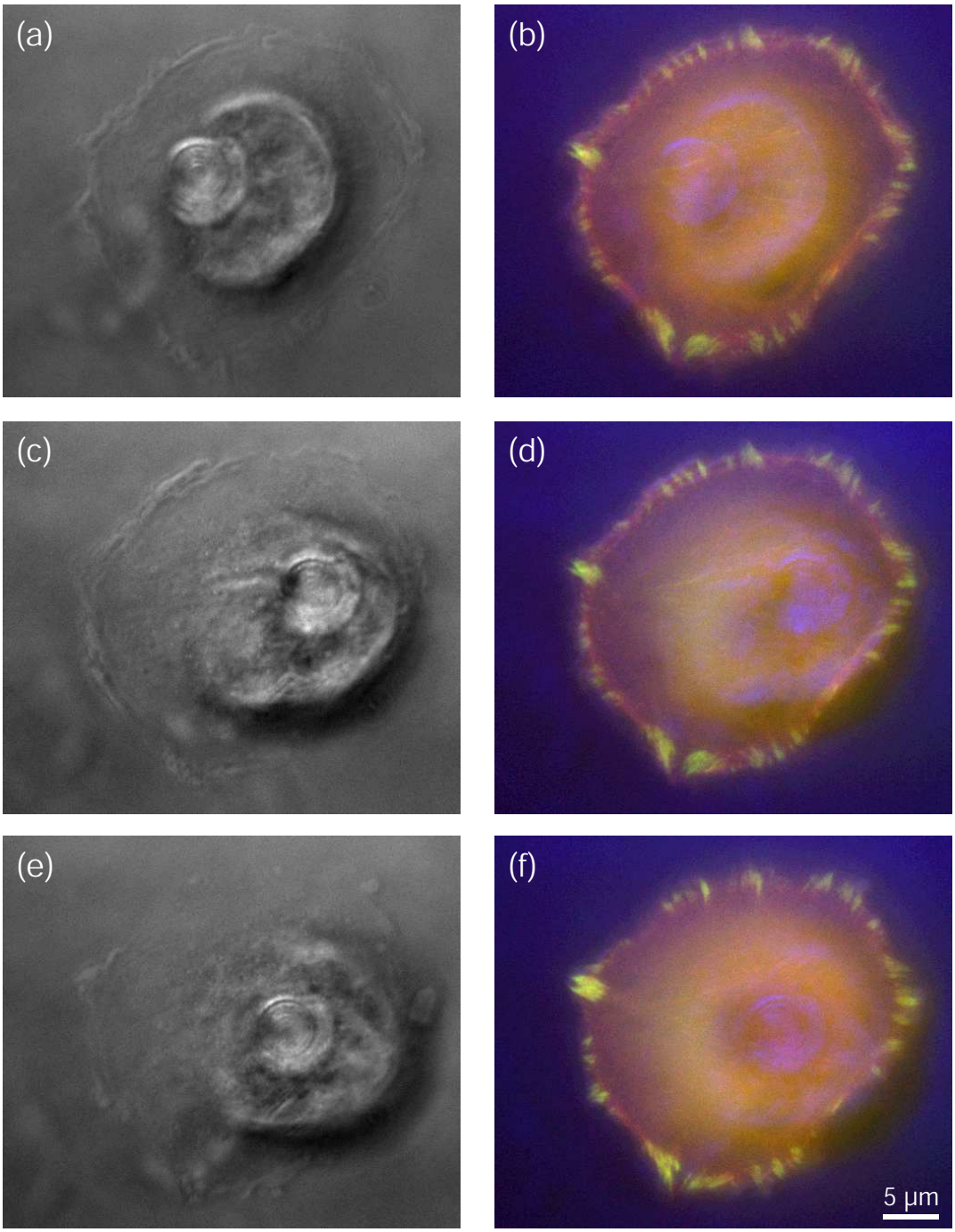

Figure 6.1: Image sequence of a cell transiently cotransfected with CFP-actin (red) and YFP-zyxin (green) that is externally sheared via a micropillar. (a,c,e) Phase contrast pictures show cell and micropillar shortly before (a), shortly after (b) and 17 minutes after pulling (c). (b,d,f) Same images (now in blue) overlayed with fluorescence data. In (c,d), one can discern the large deformations caused by shifting the pillar. However, the focal adhesions had not enough time to adjust their size to the changed loading situation. In (f), FAs on the left side of the cell have responded to the increase of internal stress: they show an increased area and a higher fluorescence intensity. The images also show a clearly visible actin cortex, but there are no stress fibers present.

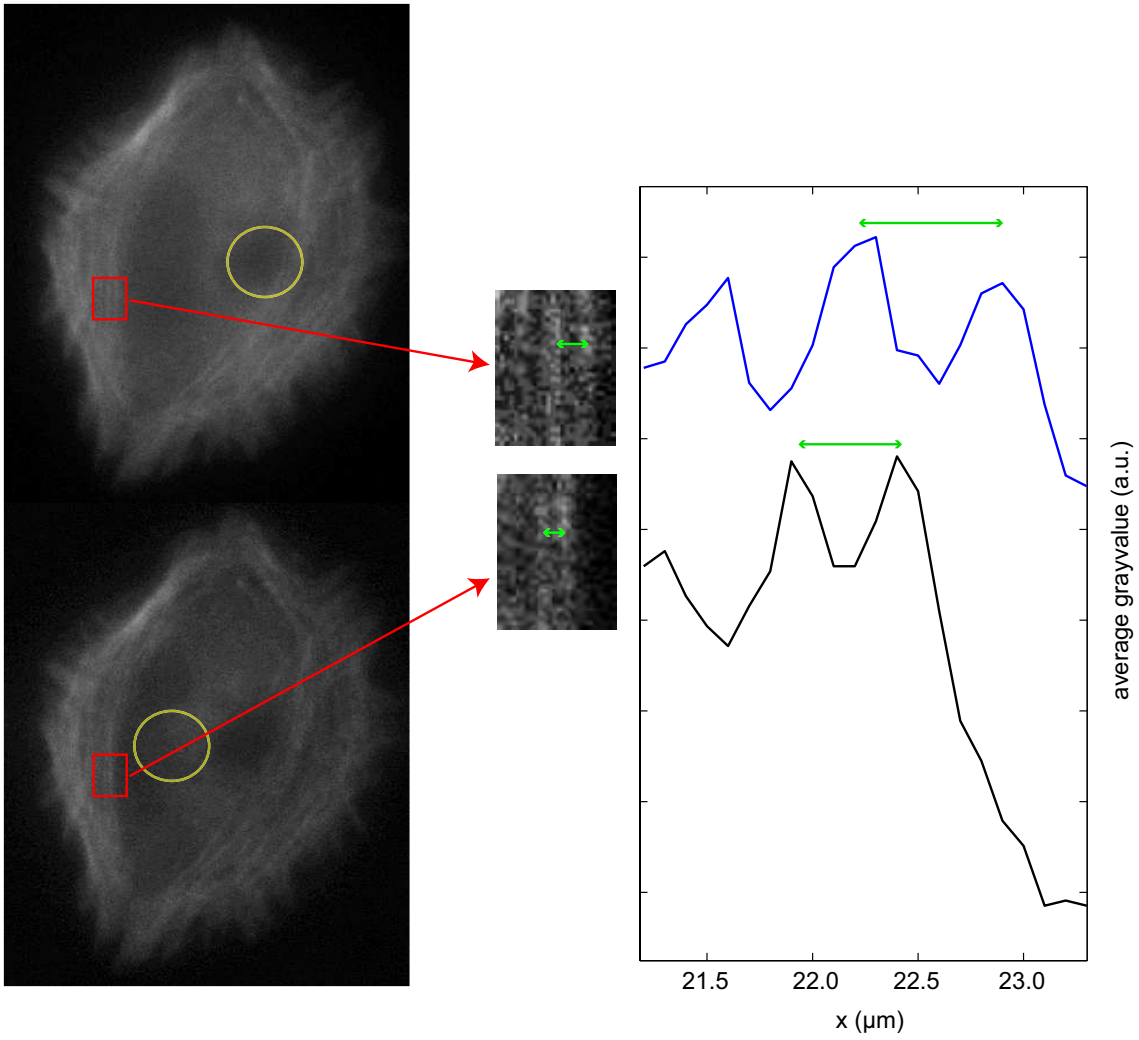

Figure 6.2: Deformation of the actin cytoskeleton due to pillar movement. The micropillar (yellow) is moved across a cell with actin stress fibers. The fluorescence micrographs depict the actin distribution before and after application of external shear. The graphs show the fluorescence intensity profile of the magnified region before (blue) and after (black) pulling. It reveals that the stress fibers are both compressed and shifted to the left. The distance between the two examined stress fibers is depicted by the green arrows.

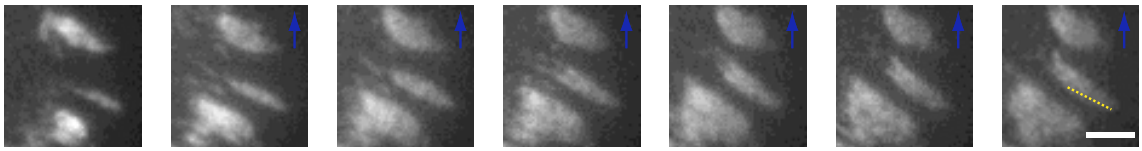

Figure 6.3: Bending of a focal adhesion due to tension oblique to its preferred growth direction. The left side of the focal adhesion cluster shown here points in the direction of the cell's nucleus. Starting with the second frame, an external force was applied to the cell pointing toward the upper side of the images (indicated by the blue arrows). As a result, the focal adhesion growth deviates from its major axis. The yellow dotted line in the last frame depicts the position of the focal adhesion's major axis in the first frame. Pictures were taken 6 minutes apart, and the scale bar is 2 µm long.

To examine the effect of the micropillar manipulation on cells that do have actin stress fibers, some experiments were conducted on cells 24 hours after plating. An example of this is shown in Figure 6.2. It demonstrates how the actin cytoskeleton is deformed by the external shear, i.e. how the applied force is transmitted through actin stress fibers and cortex. Stress fibers in the compressed region of the cell (see Figure 6.2 magnification) are shifted to the left and brought closer together, while the spacing between stress fibers on the other side of the cell is increased.

6.2 Bending of Focal Adhesions

Another interesting aspect of the conducted shear experiments was the fact that force was not always applied parallel to the preferential growth direction of FAs, but sometimes at oblique angles to it. This allowed to study the flexibility of FA clusters as a reaction to torque.

A slight deviation from the original growth direction upon force application into a different direction was observed in some experiments. An example is shown in Figure 6.3. There, a focal adhesion was subjected to an external force oblique to its major axis. As a result, the front end of the FA shifted its growing direction to the right, leading to a slightly curved FA cluster. However, only the position of newly added adhesion proteins was affected. Paxillin molecules that were already in place did not shift noticeably. Thus, the effect on the FA was rather limited.

Similar events were observed regularly for focal adhesions oriented obliquely to the external shear. On the one hand, they did ensure that the respective FA was affected by the applied force. On the other hand, they did – as the effect is only tiny (a deviation of the FA's major axis of at most 15°) – not interfere with a quantitative evaluation of FA dynamics, which was based on a one-dimensional treatment of the focal adhesions (see chapter 7).

These findings indicated already what was later confirmed by detailed analysis of focal adhesion dynamics and intensity profiles along their major axes (see chapter 7): The part of the FAs pointing towards the cell center reacted to applied force by integrating new adhesion molecules in the direction of applied force, while the FA rear was relatively stationary and inactive.

6.3 Interaction with Micropillars

6.3.1 Cells Crawling up the Micropillars

In order to promote adhesion between observed cells and the micropillar touching their dorsal side, the pillar was coated with fibronectin (see section 3.2.1), while the glass substrate was not functionalized at all. This arrangement proved to be effective in most cases, but in some, it led to an undesired, but remarkable behavior of the cells: They detached from the glass bottom and used the micropillar to climb up to the chemically more attractive PDMS pillow. In order to prevent this, the micropillar was left on the dorsal side of the cells less that 18 minutes before it was shifted laterally. Yet, in some experiments, the cells still left the glass bottom.

Figure 6.4 shows an image sequence of a cell crawling up a micropillar. In the first frame, which was taken directly after lowering the micropillar onto the cell, the latter is still undisturbed and firmly adhered to the glass bottom. The fluorescence of the paxillin molecules in the cytoplasm is close to the focal plane and symmetrically oriented around the nucleus. The cell's preference for attachment to the PDMS pillow over staying on the glass surface becomes evident already after 12 minutes: the cell starts to disassemble focal adhesion clusters on the glass substrate. Furthermore, the cytoplasm starts to be oriented more upwards, as revealed by a big amount of fluorescence that is out of focus. This becomes more obvious when the pillar is moved to the right after 16 minutes and the out-of-focus cytoplasmic fluorescence moves with it. In the following hour, the cell gradually removes focal adhesions from the glass bottom while the blurred fluorescence in the upper right corner of the images increases. The last image was taken with its focal plane on the PDMS pillow and reveals that the cell has indeed established focal adhesion clusters up there.

6.3.2 Adhesion to the Micropillar

As motivated in the previous section, cells were only given 14 to 18 minutes to connect to the micropillar before it was shifted laterally. This procedure raised the question whether the REF-52 fibroblasts were able to form stable adhesion clusters to the micropillar within this time frame under the given experimental conditions. Otherwise, parameters like the cell medium, the FBS concentration, or the functionalization of the PDMS would have had to be varied in order to ensure strong adhesion and thus effective transmission of external shear to the cytoskeleton.

As shown in Figure 6.5, there were indeed cases where FA clusters on top of the micropillars were observed. This image sequence depicts a cell sheared thrice by lateral micropillar movement. Just before the first of these external manipulations, a faint fluorescence ring is visible around the pillar, indicating adhesion clusters in the progress of formation. This fluorescence is evidently increased after the application of external shear, nicely demonstrating force-induced FA growth. When the micropillar is moved for the second and third time, these FA clusters move with it, proving the firmness of their adhesion.

Focal adhesion clusters on the top of the micropillar similar to the ones shown here were observed in only four instances. Yet, it can be assumed that stable adhesion to the micropillar occurred more often than this: Either on the sides of the pillar, which would only be detected as a gleaming around it, or on top of a pillar which was too far above the focal plane to be spotted.

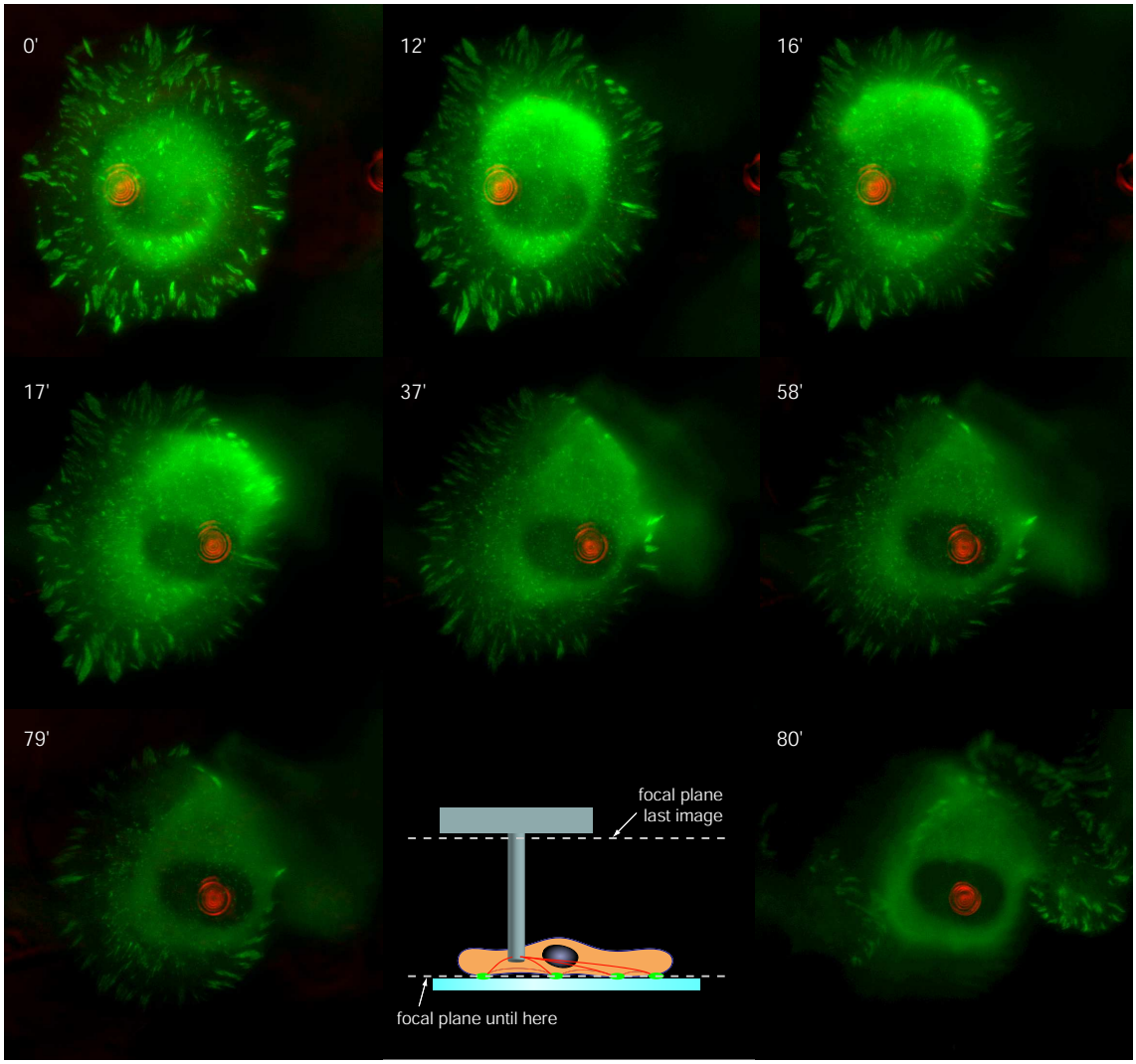

Figure 6.4: Image sequence of a cell crawling up a micropillar. Paxillin fluorescence is shown in green, and phase contrast images are overlayed in red. The focal plane is just above the glass substrate for all images except the last one, where it is on the PDMS pillow. The sequence shows how the cell uses the micropillar to move from the unfunctionalized glass bottom to the fibronectin-coated PDMS pillow. In the first frame, the cell is still undisturbed and firmly adhered to the bottom: The fluorescence of the cytoplasm is in focus and symmetrically distributed around the nucleus. Already after 12 minutes, the cytoplasm of the observed cell starts to orientate more upwards, indicated by a big amount of fluorescence that is out of focus. This becomes more obvious when the pillar is moved to the right after 16 minutes and the out-of-focus cytoplasmic fluorescence moves with it. Over the next frames, the cell disassembles adhesion clusters on the substrate. As visible in the last frame with its focal plane on the PDMS pillow, FA clusters were established on its surface. The diameter of the micropillar is 5 µm.

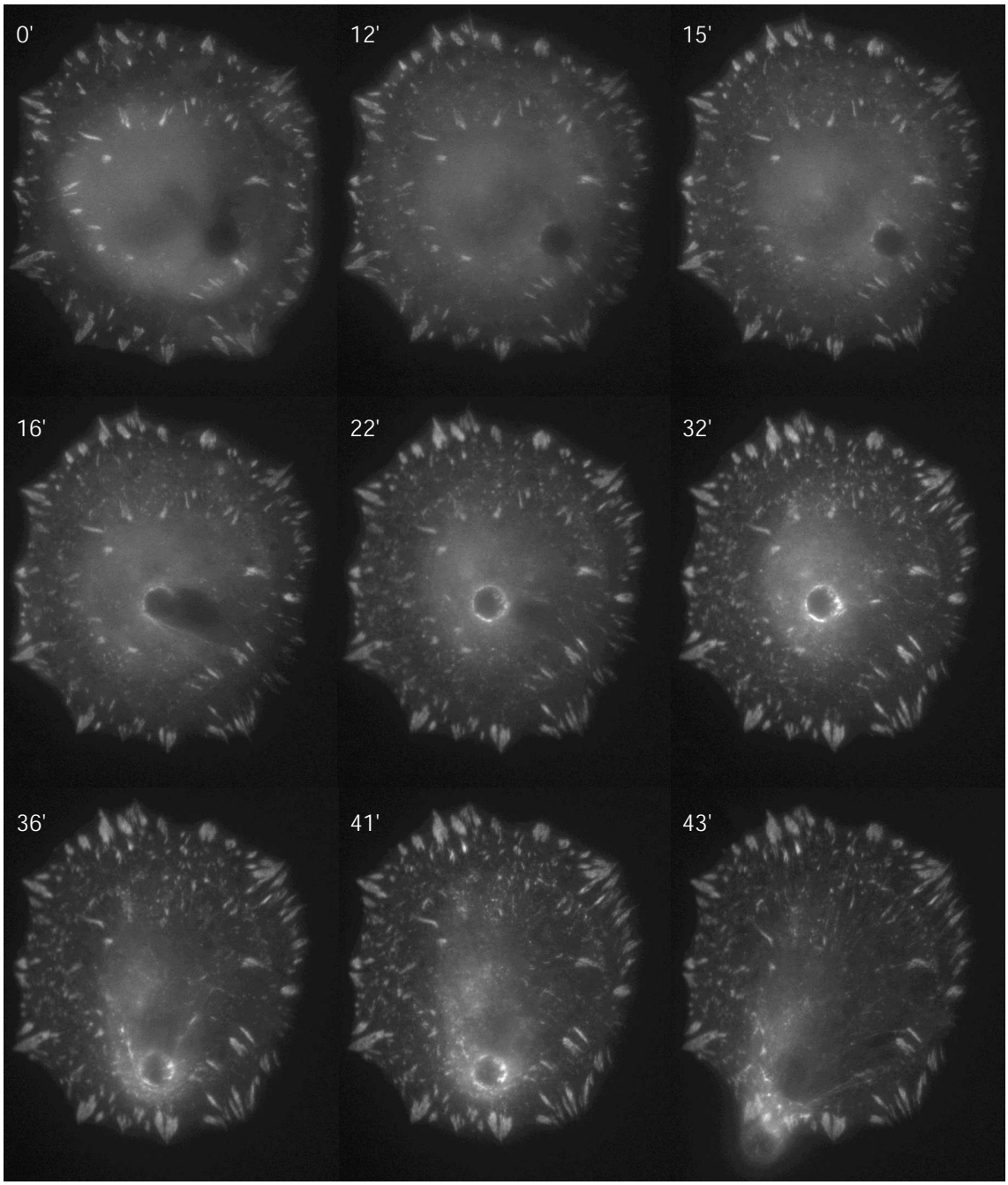

Figure 6.5: Focal adhesion clusters on the micropillar. Image sequence showing the paxillin fluorescence of a cell sheared three times by a micropillar. In the second and third frame, the paxillin molecules start to accumulate around the circumference of the pillar. These small adhesion clusters grow rapidly after a shear force is applied to them (see second row of images). They even stay on the pillar after two more lateral pillar shifts, indicating a strong adhesion to the biofunctionalized PDMS. Note that the top of the pillar is in the focal plane of the FAs on the glass substrate. The diameter of the micropillar is 5 µm.

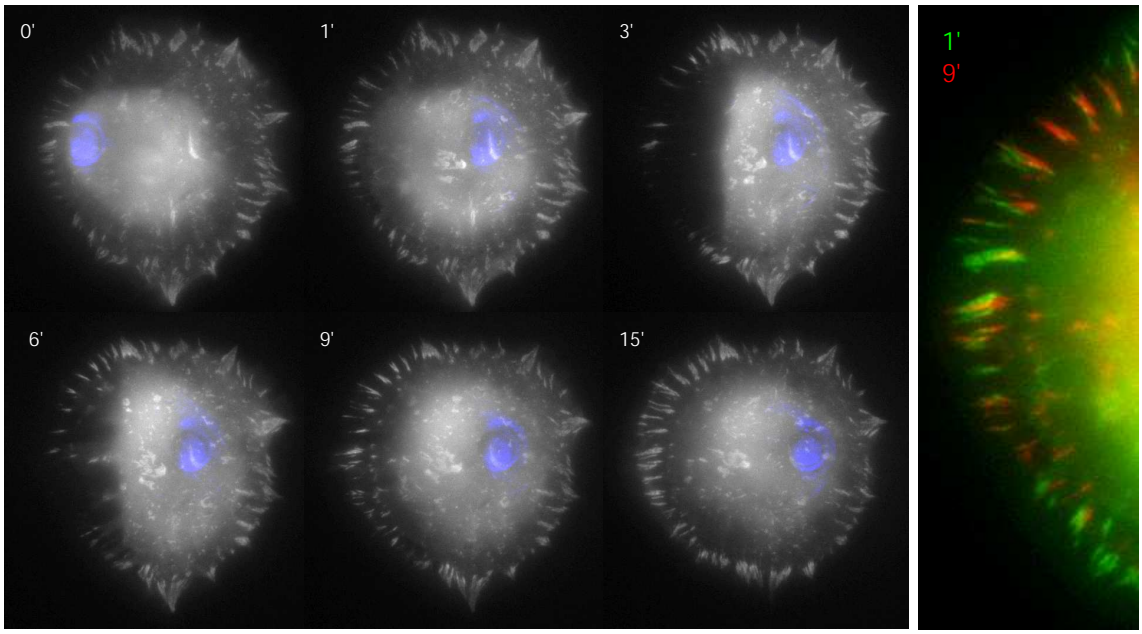

Figure 6.6: A cell backtracking its footsteps. The images were taken starting 3 hours after seeding in medium containing 1% FBS. Fluorescent paxillin is shown in gray, and the phase contrast channel depicting the micropillar is overlayed in blue. As a result of the lateral pillar movement (second frame), the left half of the cell is detached from the substrate. Surprisingly fast and accurately, and in spite of the presence of the pillar, the cell re-attaches at the positions where it had formed FA clusters before being ripped off the surface. This suggests that the cell had deposited an extracellular matrix with specific adhesion-promoting molecules (such as fibronectin) underneath itself, most of which stayed on the substrate during the shear. The panel on the right hand side shows a magnified overlay of the affected region before (green) and after (red) detachment. The diameter of the micropillar is 5 µm.

6.4 Cells Backtracking Their Footsteps

A further unknown experimental parameter was whether or not the cells were able to secrete their own extracellular matrix within the time frame of the measurements. This question was answered by observations made on a cell 3 hours after it was seeded onto an untreated glass surface. After being partially detached from the substrate by a shear force, it subsequently re-attached at the positions where FAs had been before the external disturbance in a remarkably fast and accurate manner (see Figure 6.6). A comparison between the FA positions before and after detachment is shown in the right panel of Figure 6.6. Paxillin fluorescence before the external disturbance is shown in green, and the fluorescence afterwards is overlaid in red.

Similar events were observed in several experiments. This led to the conclusion drawn that the REF-52 fibroblasts were indeed capable of secreting a functional ECM (including adhesion promoting ECM proteins such as fibronectin) underneath themselves within hours. These findings are in accordance with recent research about fibronectin secretion of this cell line (Dragovits, 2006).

6.5 Mortality statistics

It should be mentioned that none of the cells survived the experiments. In fact, most of them died either after the pillar was lowered onto their dorsal side or directly after it was moved laterally across the cell. This was attributed to a course handling of the micropillar. On the other hand, if the manipulation through the pillar was too subtle, the cell in question showed no discernible reaction. This was the case in about 40% of the experiments.

It proved to be very challenging to find the right balance between the two extremes and shear the cell enough to provoke a reaction yet not too much to ensure its survival. Thus, only 13% of the examined cells survived at least one lateral micropillar movement and displayed FA remodeling as a reaction. One third of these cells could not be analysed because the image quality was not sufficient to distinguish single focal adhesions over an extended period of time. This was in most cases due to a shift of the focal plane – for experiments done prior to the implementation of the laser auto focus.

This chart shown below is meant to give the reader an impression of the performance and productivity of the method described here.

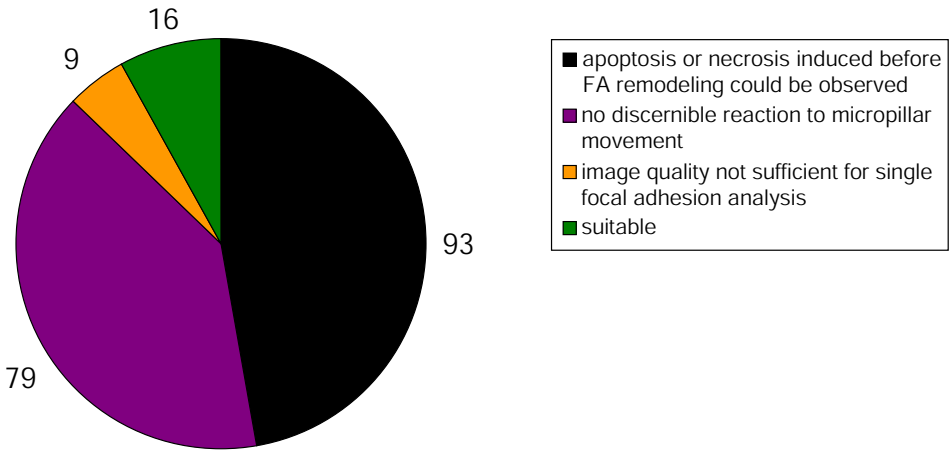

Figure 6.7: Chart depicting the success rate of the conducted experiments. Numbers indicate the number of examined cells in the respective category.

7 Focal Adhesion Remodeling Induced by External Shear Stress

The following chapter describes the results obtained on FA remodeling induced by external shear stress. As explained before, our approach to manipulate the intracellular stress – and thus the tension sensed by individual FAs – was to move a cell-attached micropillar laterally across the cell. The affected FA clusters reacted to this external stimulus within several minutes. After at most 30 minutes, the cells had usually adapted to the new loading situation, and the remodeling of the FAs had saturated. If the respective cell survived until then and showed no signs of beginning apoptosis, the micropillar was moved again in order to affect more FAs and generate more data. This procedure was repeated up to four times.

Figure 7.1 shows such a double pull experiment in which a fibroblast was first subjected to stress in x-direction and then in y-direction. The phase contrast pictures show the deformations caused to the cell body and the position of the micropillar. Comparing the latter to the position of its neighbor (not shown), the externally applied forces were calculated. Their temporal development is shown in the inset, and red arrows in the phase contrast images indicate the force at the time the pictures were taken.

After each lateral movement of the micropillar, the system was left alone and the subsequent relaxation of the external force was observed (see inset of Figure 7.1). Resulting from the manipulation of the intracellular stress, the FA assembly of the cell underwent a remodeling (compare Figure 7.1 d-f and Figure 7.2). We found increased fluorescent paxillin intensity and elongation of FAs in regions subjected to stretching, such as the lower right region of the cell in Figure 7.1 e and the lower left corner in Figure 7.1 f. On the other hand, FAs in regions with decreased internal stress showed only a loss of fluorescence and no discernible variation of their length (compare upper half of the cell in Figure 7.1 f and left hand side of Figure 7.1 e).

This distinct behavior, an elongation and increased fluorescent intensity for stressed FAs on the one hand, and isotropic intensity loss for relaxed FAs on the other, was consistently observed in all conducted experiments.

7.1 Focal Adhesion Dynamics Under External Shear

A more detailed analysis of the FA remodeling is presented in Figure 7.2. Here, kymographs are shown that are derived from the FAs inside the orange (Figure 7.2 a-d) and yellow (Figure 7.2 e-h) boxes in Figure 7.1. Using the image analysis algorithms described in Chapter 4, the front and back position of the FAs were detected for each frame (Fig-

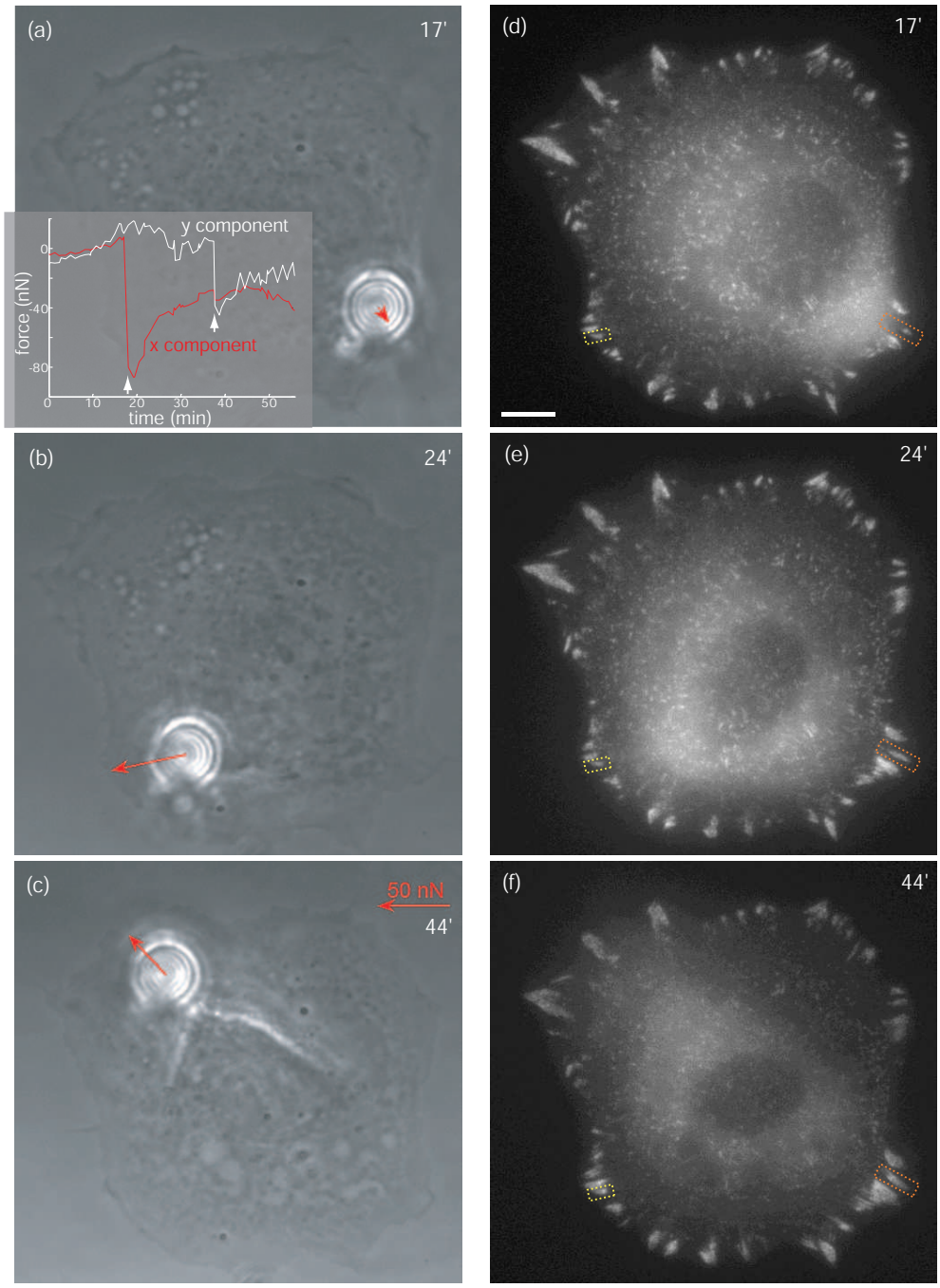

Figure 7.1: Double pull experiment. Phase contrast pictures show cell and micropillar shortly before lateral pulling (a), after first pulling (b) and after second pulling (c). The red arrow indicates the force exerted by the micropillar which was moved manually twice (at 18' and 37') and left to relax afterwards. (d-f) Fluorescence micrographs showing the resulting distribution of YFP-paxillin. Force-induced growth (yellow and orange box) and shrinkage (yellow box) of FAs is observed (for a detailed analysis see Figure 7.2). Regions with decreased internal stress display lower intensity: See upper half of (f) and left hand side of (e). The inset depicts the force development computed from the pillar position compared to that of its neighbor. Arrows mark the times where the pillar was moved manually. Relaxation of external load can nicely be seen. The bar is 5 µm.

ure 7.2 b,f solid lines). To reduce the high errors stemming from the temporal derivative, a cubic smoothing spline fit was applied to the position data (Figure 7.2 b,f dashed lines) before calculating the velocity of the back and front of the FAs (Figure 7.2 c,g).

The resulting position and velocity data of the FA back and front reveal distinct features for the two cases: Upon stretching, both front and back of the FA move in direction of the applied force, but the front moves at a much higher velocity, leading to a net growth of the FA (compare Figure 7.2 b,c). Upon compression however, the observed FA does not shrink noticeably, but merely stops growing and loses intensity (Figure 7.2 e-g). The latter process showed to be reversible: The growth of the FA was re-initiated later by an application of a force in the opposite direction.

These characteristic, distinct reactions of FAs to stretching and relaxation were observed in all conducted experiments. Compare Figure 7.4 for an overview of selected FA kymographs. The reversibility of these processes has been confirmed in several of the measurements: Growth was induced in stationary FAs and subsequently stopped again by lowering the intracellular tension (see e.g. Figure 7.4 k,l) and vice versa (Figure 7.4 b,m).

As explained in section 4.2.1, the measured total external force was projected onto the major axis of the respective FA to reflect the relative amount of stress applied in its preferential growth direction (Figure 7.2 d,h). Thus, positive values mean stretching and negative values compression of the FA in question. Following each lateral movement of the pillar (depicted by vertical dashed lines in Figure 7.2), these force curves depict consistently a relaxation of the system. Interestingly, the velocity curve of the front of the stretched FA follows the force curves down to its small irregularities which are possibly due to intrinsic cell movement (gray arrows).

Note that the exact distribution of the externally applied stress to the different FAs is unknown and changes after each manual movement of the micropillar. Thus, the projected forces after pillar movement can not be compared to the ones before. This means, a proper scaling of the forces can only be assumed between the dashed lines in Figure 7.2. This explains for example that the second manual pillar movement barely influences the contact depicted in the left column of this figure, but significantly affects the contact in the right column – although the nominal value of the projected forces could mislead to think otherwise.

7.2 Intensity Profiles Along Stressed Focal Adhesions

A closer look at the intensity distribution of remodeling FAs reveals even more substantial differences between stretched and relaxed focal adhesions: Figure 7.3 shows a comparison of the intensity profile along the major axis of a stretched (a-d) respectively relaxed (e-h) FA before and after force application. Times of stretching and compression are marked by a white respectively black arrow.

A temporal averaging over the blue and green boxes results in the intensity profiles before (blue) and after (green) external shear (Figure 7.3 b,f). The difference between the two shows where exactly proteins have moved into or out of the FA as a response to the changed loading situation (Figure 7.3 c,g).

In the case of the stretched FA, this analysis reveals a Gaussian distribution that is centered over the former front of the FA. This means that only there, the FA reacts to the increased stress. A subtraction of the averaged profile before stretching from each row of

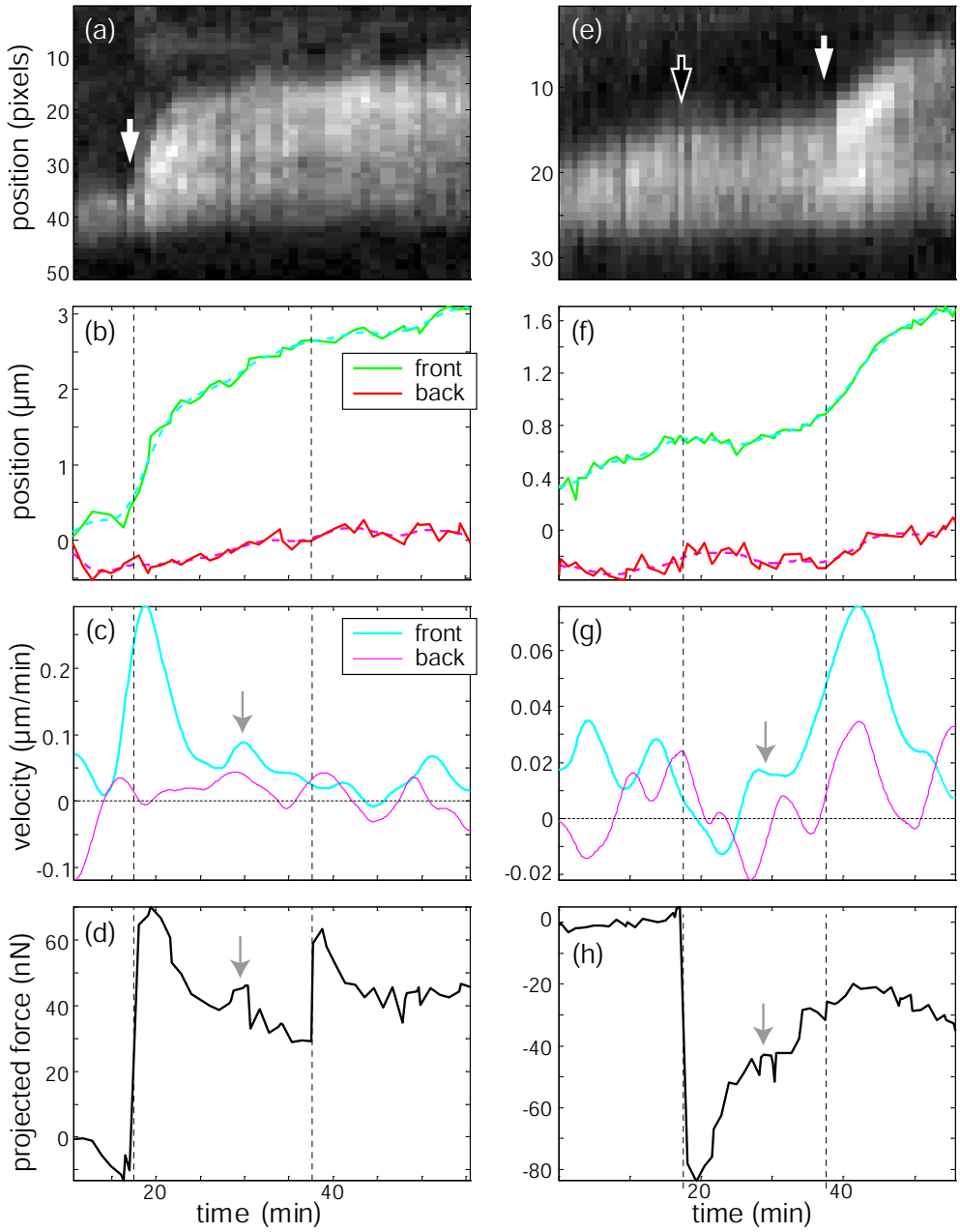

Figure 7.2: Dynamics of a stretched (a-d) and a relaxed (e-h) FA. Kymographs obtained from the FAs inside the orange (a) and yellow (e) box in Figure 7.1 show the temporal development of the FAs after external manipulation. Times of externally induced stretching and compression are denoted by white and black arrows in the kymographs and by dashed lines in the graphs below. The calculated positions (b,f) and velocities (c,g) of back and front reveal that upon stretching, the FA front moves much faster in the direction of applied force than the back, leading to a growth of the FA (b,c). However, the compressed FA does not shrink, but merely stops growing and loses intensity (e-g). The total external force calculated from the micropillar deflection is projected onto the direction of the major axis of the respective FA such that positive values mean stretching and negative values compression of the FA (d,h). This projected force scales similarly to the velocity of the FA front. Even small deviations in the force curve are matched by corresponding peaks in the velocity curves (see gray arrows).

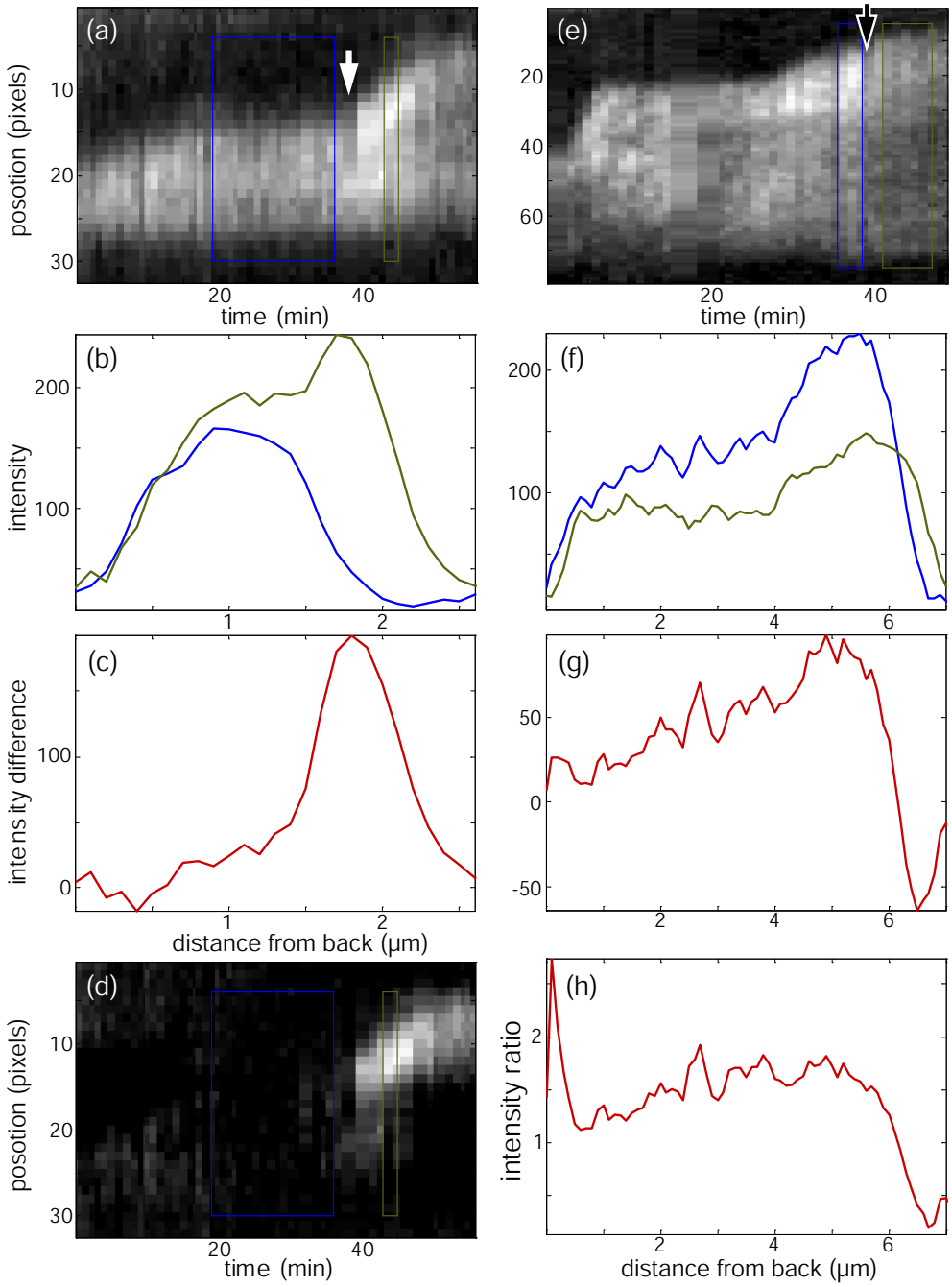

Figure 7.3: Influence of stretching and compression on paxillin fluorescence intensity profiles along a growing (a) and disassembling (e) focal adhesion. The green and blue boxes in the kymographs (a,e) depict the region over which the corresponding profiles shown in (b,f) are averaged. The distribution of proteins that have moved into the FA as a response to increased or decreased stress can be clearly seen if one subtracts the profile before from the one after the respective manipulation (c,g) or computes the ratio of the two (h). This reveals that only the very front of the stretched FA responds to the external stimulus, whereas the relaxed FA loses plaque proteins over its whole length. The region where new proteins are inserted upon stretching displays a Gaussian distribution which diffuses over time (see (d), a subtraction of the profile before stretching from the original kymograph).

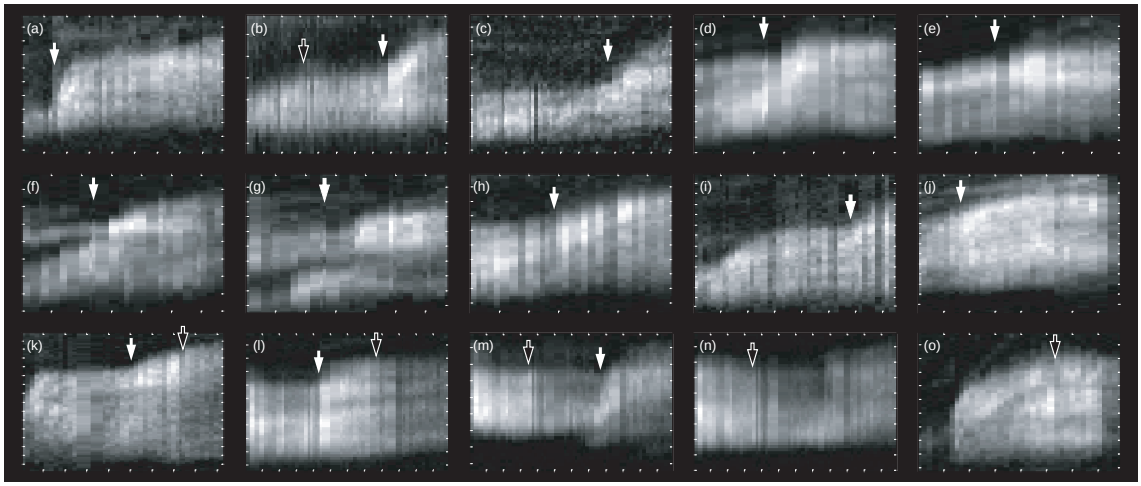

Figure 7.4: Compilation of FAs that have been stretched (white arrows) and compressed (black arrows). In the kymographs, ticks denote 5 minutes on the x-axes and 5 µm on the y-axes. Upon stretching, FAs elongate and display consistently a spatially very confined integration of new paxillin molecules at their front, whereas compression results in stagnation of length and fluorescence loss over the whole FA.

the original kymograph depicts nicely how this Gaussian peak diffuses over time (compare (Figure 7.3 d).

Compression evokes a distinctly different response. Instead of reacting only at the front as its stretched counterpart, the relaxed FA loses intensity over its whole length. This becomes most obvious when computing the ratio of intensities before and after compression which stays rather constant (compare (Figure 7.3 h) – except for deviations at the very front and back that are due to overall movement of the FA.

Hence, the insight gained from this investigation is that in the case of the stretched FA, only its very front responds to the external stimulus, whereas the relaxed FA loses plaque proteins over its whole length. In Figure 7.4, we show an overview of kymographs collected from seven different cells to demonstrate how these characteristic reactions apply qualitatively to all examined cells.

The Gaussian distributions seen in the kymographs of all stretched FAs have not been reported in literature and hence deserve some more attention. Figure 7.5 a displays such paxillin influx profiles computed from kymographs shown in Figure 7.4. The Gaussian peaks consistently seen in these profiles display a very variable width. This raises the question which factors determine the broadness of this distribution.

One possible candidate is the length of the respective FA. However, a plot of the full width at half maximum of Gaussian fits to the influx profiles vs. the length of the corresponding FA does not support such an assumption: The linear fit of these data does not show a proportionality.

This suggests that the width of the region where new adhesion molecules are inserted depends on a variable that was not measured, most likely the absolute amount of applied stress and its distribution along the FA.

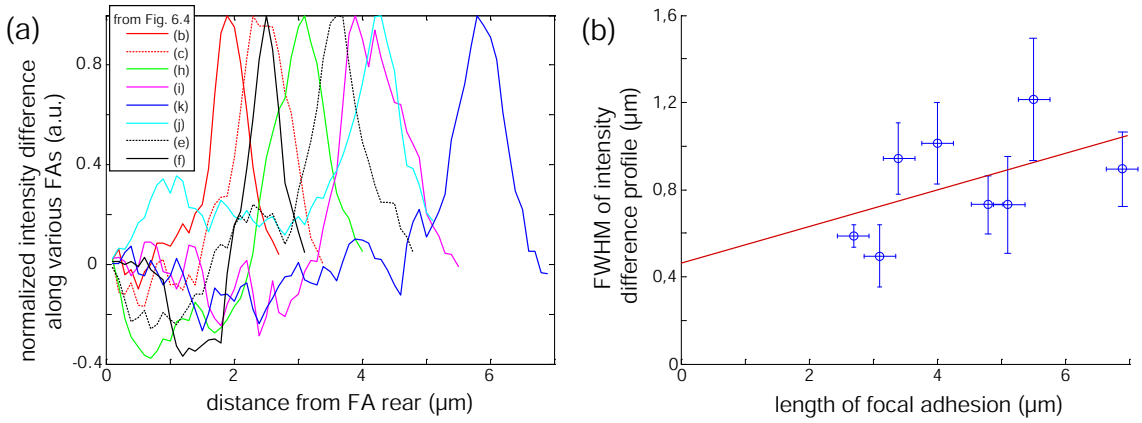

Figure 7.5: (a) Graph showing the difference in paxillin fluorescence before and after stress application for several focal adhesions. The intensity is normalized such that the maximal difference is 1. The legend indicates to which kymograph in Figure 7.3 the respective profile corresponds. (b) Plot of the full width at half maximum of the depicted intensity profiles versus the length of the corresponding FA with error bars. The red line represents a linear fit to these data.

8 Comparison Between Simulation and Experiment

In order to estimate the force distribution from the micropillar to distinct focal adhesions, simulations of stress propagation through the actin cytoskeleton were employed (Paul et al., 2007). As illustrated in Figure 8.1, these simulations were used to compare experimentally measured FA areas to simulated forces exerted at these points.

The first row of Figure 8.1 shows segmented fluorescence images of a cell directly before and 30 minutes after lateral movement of the micropillar to the left. The anchor points in the simulation (see Figure 8.1 b,e) were positioned according to the positions of the focal adhesion clusters extracted from these images. They are depicted as red circles in Figure 8.1 b and e. The diameter of these circles represents the force applied by the cytoskeleton to the respective anchoring point.

As it was found that the force transduced by a focal adhesion is proportional to its area (Balaban et al., 2001; Tan et al., 2003), we compared these two quantities: The forces applied to the simulated anchoring points were compared to the areas of the respective focal adhesions in the experiment (see Figure 8.1 c). The two quantities matched fairly well for the situation before external shear.

However, the comparison between the focal adhesion areas 30 minutes after external stress application and the forces of the correspondingly sheared cell model was not as convincing in detail (see Figure 8.1 f). The deviations between the two graphs are too significant to rely on this kind of simulations to estimate the force transmitted through the cytoskeleton to certain focal adhesions.

For a more detailed interpretation of these results, refer to Paul et al. (2007).

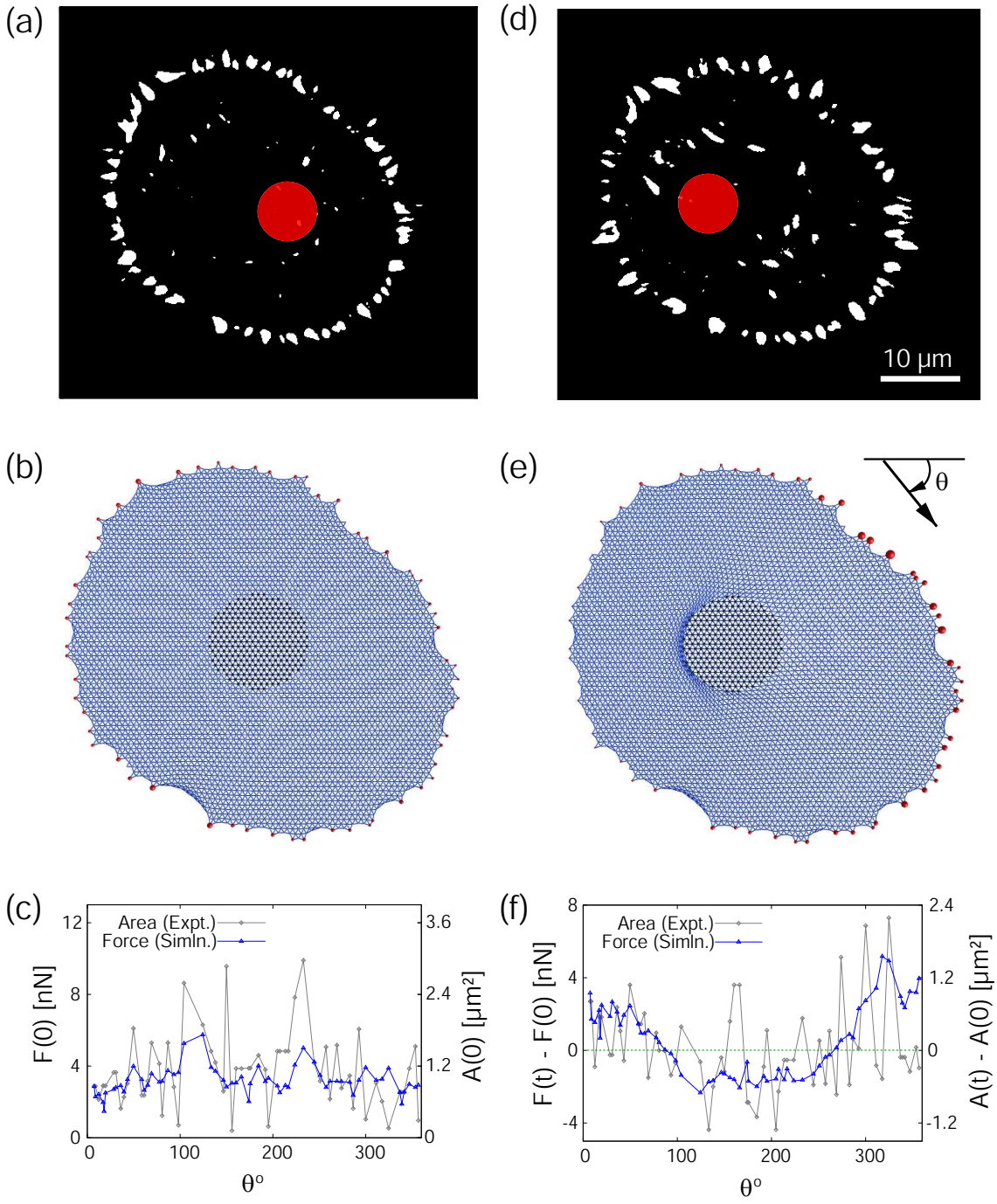

Figure 8.1: Simulation of propagation of mechanical stress through the actin cytoskeleton towards focal adhesions. The experimental data of a cell before (a) external force application display the area and position of the FAs. Only the FA positions were fed into a the simulation, and the respective areas were calculated (b). The changes in the FA assembly 30 minutes after external shear measured in the experiment (d) were compared to the results of an analogous stress application in the simulation (e). Plots of the measured areas and simulated forces are shown in (c) and (f) for the two timepoints. Taken from Paul et al. (2007)

Part IV

Conclusions

9 Discussion

9.1 Dynamics of Focal Adhesion Molecules Under External Shear

We successfully induced FA assembly and disassembly by shearing cells with microfabricated, flexible polymer pillars. Our results are in accordance with those obtained in previous studies (Riveline et al., 2001; Zaidel-Bar et al., 2005) but go beyond them in their temporal and spatial resolution.

Our studies were performed on live cells, and the FBS concentration in the medium was carefully and successfully chosen to keep them in an intermediate state where they were neither starved nor completely spread. Hence, their metabolism was ensured to be very active and responsive to both external stretching and compression - unlike in previous experiments by Riveline et al. (2001) where cells were serum-starved and thus not able to produce mature FAs on their own.

Furthermore, the examined cells displayed a homogeneous actin cortex without stress fibers, allowing to estimate the stress distribution inside the cell.

Focal adhesions that were subject to increased lateral stress displayed a distinct growth behavior. The front end moved at a velocity of up to 0.3 µm/min proportional to and in direction of the applied stress. The rear of the observed focal adhesions was consistently rather stationary; it showed very little reaction to applied forces. Thus, externally stretched FAs displayed a net growth along their major axis, a finding consistent with previous studies (Riveline et al., 2001).

On the other hand, we found that relaxation of FAs causes only negligible shortening, but may stop ongoing growth (compare Figure 7.2 f,g).

A comparison of the intensity profile before and after pulling yielded interesting insight into the exact position of newly inserted plaque proteins (see Figure 7.3 c) and their dynamics. Stretched focal adhesions showed an influx of plaque proteins only in their front region. The profile of this additional fluorescence intensity displayed Gaussian distributions with FWHMs between 0.5 µm and 1.5 µm.

Conversely, the FA remodeling following a decrease of internal prestress showed to be isotropic: a uniform loss of plaque proteins along the whole length of the respective FA was observed (compare Figure 7.3 h).

All these processes have been found to be reversible: We have induced growth in stationary FAs and subsequently stopped it again by lowering the intracellular tension (see e.g. Figure 7.4 k,l) and vice versa (Figure 7.4 b,m).

9.2 Impact on Theoretical Models

The presented data will help to evaluate whether the competing theories in this field describe underlying principles of mechanosensitivity correctly. The observed growth velocities, intensity profiles along FAs and their evolution over time can be compared to the predictions of the two models that deal with the dynamics of force-induced focal adhesion remodeling.

In particular, the spatially very confined influx of protein molecules into the front of stretched FAs allows to differentiate between these two models. This peculiar phenomenon seems to be more consistent with the theory presented by Besser and Safran (2006), who derive an influx proportional to the protein density gradient, which should be maximal at the FA edges (compare section 1.4.2). The theory by Shemesh et al. (2005) predicts a smoothly varying influx along a stretched focal adhesion, which has not been observed in the experiments presented here.

However, to make definitive statements about the validity of either of the theoretical models, detailed calculations of the influx profile for a given stress are needed in the framework of the respective models. These calculations should include a more realistic assumption for the stress profile along the FAs than a linear one, for example the one suggested by Aroush and Wagner (2006).

The observed disassembly of plaque proteins over the whole length of relaxed FA is so far not in accordance with either of the two theories. This might change if a non-constant stress profile was assumed (see above).

9.3 Developed Techniques

On the technical side, we have shown that single PDMS micropillars are a viable tool to laterally shear cells. We have applied forces of up to 150 nN and detected them via an algorithm developed by us (see section 4.2.1) with an accuracy down to 4 nN.

Furthermore, an automated focusing system was implemented into our setup, greatly easing the experimental procedure and enhancing the quality of the obtained image sequences.

10 Outlook

Although we gained intriguing results on force-induced FA dynamics, one drawback of the experimental method presented here is certainly that it gives no information about the strain distribution inside a particular cell. It has only been measured how much force is applied in total, and it can be assumed that this force has to be transmitted through the FAs to the substratum. But the amount of force at a particular FA can only be estimated.

One attempt of doing so was made by simulating the stress propagation through the actin cytoskeleton using a cable network model (Paul et al., 2007). As described in chapter 8, experimental data and simulation were in overall good accordance. However, a comparison between the FA areas 30 minutes after external stress application and the forces of the correspondingly sheared cell model was not as convincing in detail (see Figure 8.1 f). Had the agreement been better, these simulations could have been used to estimate the force transmitted through the cytoskeleton to certain focal adhesions.

To enhance this agreement, this model could in the future be extended to include aspects like the three-dimensional nature of the cell or the influence of the nucleus, which is clearly deformed in the experiments.

Another approach to quantify the stress transduced by specific focal adhesions is the use of flexible substrates as they were described in section 1.5. Preliminary studies on this have been performed, applying the experimental method described in this thesis to cells seeded onto polyacrylamide gels with embedded fluorescent marker beads. The strain field induced by an adherend cell caused a movement of these beads which could be observed (see Figure 10.1 a-c). This allowed to compute the responsible stress field (see Figure 10.1 d) and thus track the forces below single focal adhesions.

However, due to the softness of the gels, the cells adhered on top of them only developed very frail focal adhesions (see Figure 10.2) that were not suitable for shear experiments. It remains a task for future experiments to overcome this obstacle, for example by using stiffer gels and improving their biofunctionalization.

Future experiments could furthermore include a force feedback system that monitors applied forces in real time. This would e.g. allow to study the effect of oscillating or constant, i.e. not relaxing, stress on FA growth.

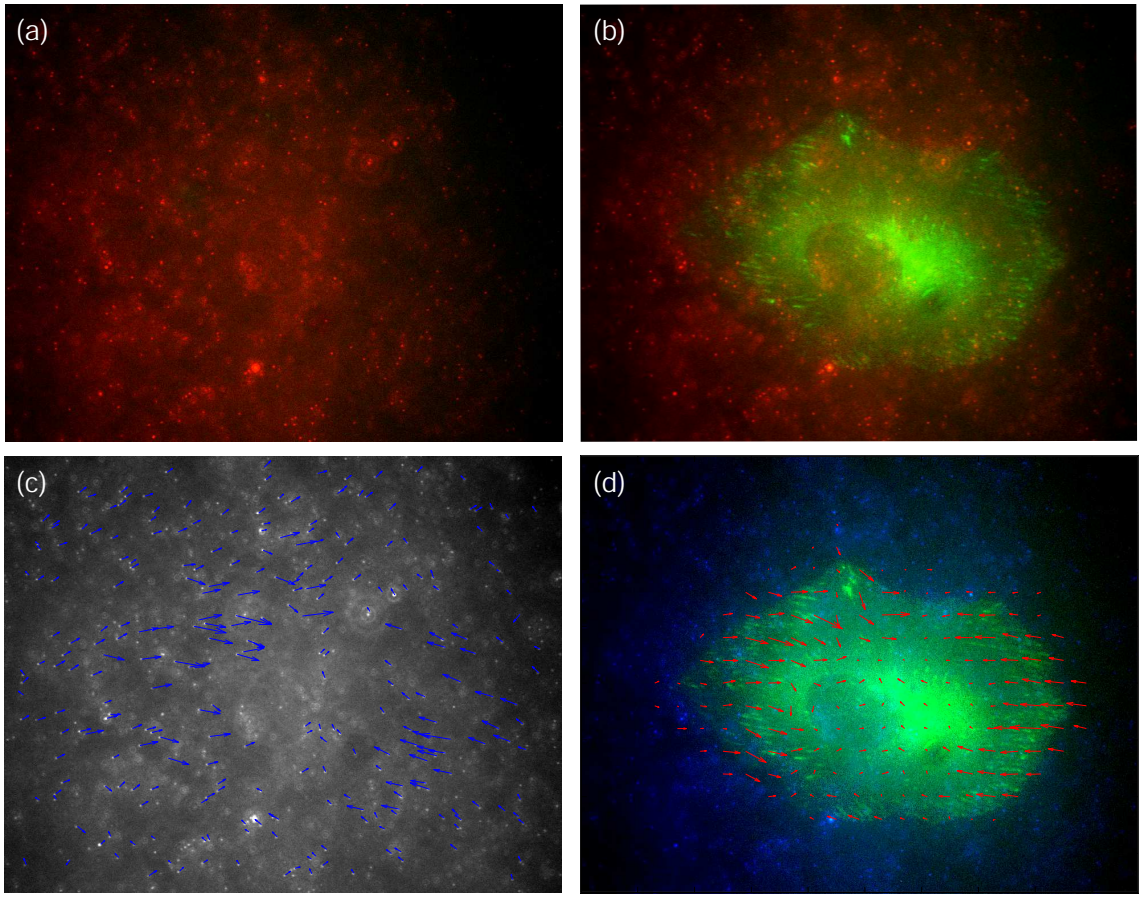

Figure 10.1: Traction force measurements with PAA gels. Panel (a) shows the fluorescent marker beads (red) embedded in a flexible polyacrylamide gel. (b) A picture taken at the same position but with a cell on top of it reveals the movement of the beads. The paxillin fluorescence of the cell is shown in green. Panel (c) shows the strain field derived from the movement of the beads, and (d) displays the computed qualitative stress field that caused this displacement. An overlay of the cell (green) demonstrates nicely that the regions of high paxillin density are also the regions where the highest stress is applied to the substrate.

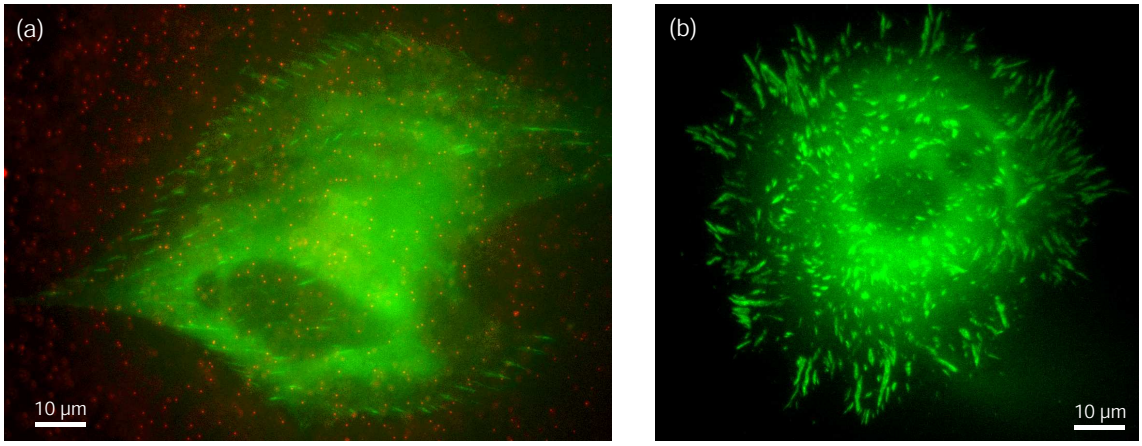

Figure 10.2: Comparison of focal adhesions on different substrates. Focal adhesions (green) on a PAA gel with embedded marker beads (red) are relatively thin and short (a) compared to those on an untreated glass substrate (b).

List of Figures

Bibliography

Alberts, B., Johnson, A., Lewis, J., Raff, M., Roberts, K., and Walter, P. (2002). *Molecular biology of the cell*. Garland Science, New York.

Aroush, D. R. and Wagner, H. D. (2006). Shear-stress profile along a cell focal adhesion. *Adv Mater*, 18:15371540.

Balaban, N. Q., Schwarz, U. S., Riveline, D., Goichberg, P., Tzur, G., Sabanay, I., Mahalu, D., Safran, S., Bershadsky, A., Addadi, L., and Geiger, B. (2001). Force and focal adhesion assembly: a close relationship studied using elastic micropatterned substrates. *Nat Cell Biol*, 3(5):466–472.

Bao, G. and Suresh, S. (2003). Cell and molecular mechanics of biological materials. *Nat Mater*, 2(11):715–725.

Beningo, K. A., Dembo, M., Kaverina, I., Small, J. V., and Wang, Y. L. (2001). Nascent focal adhesions are responsible for the generation of strong propulsive forces in migrating fibroblasts. *J Cell Biol*, 153(4):881–888.

Bershadsky, A. D., Balaban, N. Q., and Geiger, B. (2003). Adhesion-dependent cell mechanosensitivity. *Annu Rev Cell Dev Biol*, 19:677–695.

Besser, A. and Safran, S. A. (2006). Force-induced adsorption and anisotropic growth of focal adhesions. *Biophys J*, 90(10):3469–3484.

Boal, D. (2002). *Mechanics of the Cell*. Cambridge University Press.

Choquet, D., Felsenfeld, D. P., and Sheetz, M. P. (1997). Extracellular matrix rigidity causes strengthening of integrin-cytoskeleton linkages. *Cell*, 88(1):39–48.

Clark, E. A., King, W. G., Brugge, J. S., Symons, M., and Hynes, R. O. (1998). Integrin-mediated signals regulated by members of the rho family of gtpases. *J Cell Biol*, 142(2):573–586.

Davies, P. F., Robotewskyj, A., and Griem, M. L. (1994). Quantitative studies of endothelial cell adhesion. directional remodeling of focal adhesion sites in response to flow forces. *J Clin Invest*, 93(5):2031–2038.

Delano-Ayari, H., Kurdi, R. A., Vallade, M., Gulino-Debrac, D., and Riveline, D. (2004). Membrane and acto-myosin tension promote clustering of adhesion proteins. *Proc Natl Acad Sci U S A*, 101(8):2229–2234.

Dragovits, M. L. (2006). Organisation of fibronectin on nanostructured biofunctionalised surfaces. Master's thesis, University of Heidelberg.

du Roure, O., Saez, A., Buguin, A., Austin, R. H., Chavrier, P., Silberzan, P., Siberzan, P., and Ladoux, B. (2005). Force mapping in epithelial cell migration. *Proc Natl Acad Sci U S A*, 102(7):2390–2395.

Galbraith, C. G. and Sheetz, M. P. (1997). A micromachined device provides a new bend on fibroblast traction forces. *Proc Natl Acad Sci U S A*, 94(17):9114–9118.

Geiger, B. and Bershadsky, A. (2001). Assembly and mechanosensory function of focal contacts. *Curr Opin Cell Biol*, 13(5):584–592.

Geiger, B., Bershadsky, A., Pankov, R., and Yamada, K. M. (2001). Transmembrane crosstalk between the extracellular matrix–cytoskeleton crosstalk. *Nat Rev Mol Cell Biol*, 2(11):793–805.

Harris, A. K., Wild, P., and Stopak, D. (1980). Silicone rubber substrata: a new wrinkle in the study of cell locomotion. *Science*, 208(4440):177–179.

Herzog, M., Draeger, A., Ehler, E., and Small, J. (1994). *Cell biology: a laboratory handbook*. Academic Press, New York. Immunofluorescence microscopy of the cytoskeleton: douple and triple immunofluorescence.

Ingber, D. E. (1993). Cellular tensegrity: defining new rules of biological design that govern the cytoskeleton. *J Cell Sci*, 104 (Pt 3):613–627.

Ingber, D. E. (2003a). Mechanosensation through integrins: cells act locally but think globally. *Proc Natl Acad Sci U S A*, 100(4):1472–1474.

Ingber, D. E. (2003b). Tensegrity ii. how structural networks influence cellular information processing networks. *J Cell Sci*, 116(Pt 8):1397–1408.

Lo, C. M., Wang, H. B., Dembo, M., and Wang, Y. L. (2000). Cell movement is guided by the rigidity of the substrate. *Biophys J*, 79(1):144–152.

Munevar, S., Wang, Y., and Dembo, M. (2001). Traction force microscopy of migrating normal and h-ras transformed 3t3 fibroblasts. *Biophys J*, 80(4):1744–1757.

Nicolas, A., Geiger, B., and Safran, S. A. (2004). Cell mechanosensitivity controls the anisotropy of focal adhesions. *Proc Natl Acad Sci U S A*, 101(34):12520–12525.

Nicolas, A. and Safran, S. A. (2006). Limitation of cell adhesion by the elasticity of the extracellular matrix. *Biophys J*, 91(1):61–73.

Nobes, C. D. and Hall, A. (1995). Rho, rac, and cdc42 gtpases regulate the assembly of multimolecular focal complexes associated with actin stress fibers, lamellipodia, and filopodia. *Cell*, 81(1):53–62.

Paul, R., Heil, P., Spatz, J. P., and Schwarz, U. (2007). Propagation of mechanical stress through the actin cytoskeleton towards focal adhesions: model and experiment. *in press at Biophys J.*

Pelham, R. J. and Wang, Y. (1997). Cell locomotion and focal adhesions are regulated by substrate flexibility. *Proc Natl Acad Sci U S A*, 94(25):13661–13665.

Riveline, D., Zamir, E., Balaban, N. Q., Schwarz, U. S., Ishizaki, T., Narumiya, S., Kam, Z., Geiger, B., and Bershadsky, A. D. (2001). Focal contacts as mechanosensors: externally applied local mechanical force induces growth of focal contacts by an mdia1-dependent and rock-independent mechanism. *J Cell Biol*, 153(6):1175–1186.

Roos, W., Ulmer, J., Grter, S., Surrey, T., and Spatz, J. P. (2005). Microtubule gliding and cross-linked microtubule networks on micropillar interfaces. *Nano Lett*, 5(12):2630–2634.

Rottner, K., Hall, A., and Small, J. V. (1999). Interplay between rac and rho in the control of substrate contact dynamics. *Curr Biol*, 9(12):640–648.

Shemesh, T., Geiger, B., Bershadsky, A. D., and Kozlov, M. M. (2005). Focal adhesions as mechanosensors: a physical mechanism. *Proc Natl Acad Sci U S A*, 102(35):12383–12388.

Springer, T. A. (2002). Predicted and experimental structures of integrins and beta-

propellers. *Curr Opin Struct Biol*, 12(6):802–813.

Stamenovi, D. and Coughlin, M. F. (2000). A quantitative model of cellular elasticity based on tensegrity. *J Biomech Eng*, 122(1):39–43.

Tan, J. L., Tien, J., Pirone, D. M., Gray, D. S., Bhadriraju, K., and Chen, C. S. (2003). Cells lying on a bed of microneedles: an approach to isolate mechanical force. *Proc Natl Acad Sci U S A*, 100(4):1484–1489.

Thvenaz, P., Ruttimann, U., and Unser, M. (1998). A pyramid approach to subpixel registration based on intensity. *IEEE Transactions on Image Processing*, 7:27–41.

Vogel, V. and Sheetz, M. (2006). Local force and geometry sensing regulate cell functions. *Nat Rev Mol Cell Biol*, 7(4):265–275.

Wang, H. B., Dembo, M., Hanks, S. K., and Wang, Y. (2001). Focal adhesion kinase is involved in mechanosensing during fibroblast migration. *Proc Natl Acad Sci U S A*, 98(20):11295–11300.

Wang, N., Butler, J. P., and Ingber, D. E. (1993). Mechanotransduction across the cell surface and through the cytoskeleton. *Science*, 260(5111):1124–1127.

Wehrle-Haller, B. and Imhof, B. (2002). The inner lives of focal adhesions. *Trends Cell Biol*, 12(8):382–389.

Zaidel-Bar, R., Ballestrem, C., Kam, Z., and Geiger, B. (2003). Early molecular events in the assembly of matrix adhesions at the leading edge of migrating cells. *J Cell Sci*, 116(Pt 22):4605–4613.

Zaidel-Bar, R., Kam, Z., and Geiger, B. (2005). Polarized downregulation of the paxillin-p130cas-rac1 pathway induced by shear flow. *J Cell Sci*, 118(Pt 17):3997–4007.

Zamir, E. and Geiger, B. (2001). Molecular complexity and dynamics of cell-matrix adhesions. *J Cell Sci*, 114(Pt 20):3583–3590.

Danksagung

Diese Arbeit wäre nie zu dem geworden, was sie jetzt ist, wenn ich nicht Unterstützung von vielen Seiten erhalten hätte. Daher möchte ich diese Möglichkeit nutzen, den Menschen zu danken, ohne die die letzten dreieinhalb Jahre nicht so positiv verlaufen wären.

Zuallererst ist dabei Joachim Spatz zu nennen, der mich in seiner Gruppe aufgenommen hat und mir dieses interessante Projekt anvertraut hat. Seine Unterstützung hat es mir ermöglicht, meine Arbeit frei von finanziellen Zwängen zu verfolgen und sie auf verschiedenen Tagungen zu präsentieren. Vielen Dank dafür!

Herrn Professor Horner gilt mein Dank für die Übernahme des Zweitgutachtens und für sein Interesse an meiner Forschung.

Enorm wichtig waren für mich die Diskussionen mit Ulrich Schwarz und Achim Besser, die mir in verschiedenen Stadien meiner Arbeit wertvolle Anregungen gegeben haben.

I thank Benny Geiger for the enlightening discussions, the cells and the vectors. His colleague Zvi Kam helped to plan the implementation of the Laser Auto Focus. I am very grateful for that.

Dank gebührt auch den Mitarbeitern am Physikalisch-Chemischen Institut, die mich im Laufe meiner Arbeit unterstützt haben: Die Zusammenarbeit mit Herrn Weis und seinen Mitarbeitern aus der Feinmechanik-Werkstatt war reibungslos und außerordentlich fruchtbar. Ohne ihre Beratung und einwandfreie Arbeit wären viele meiner Projekte nicht möglich gewesen. Herrn Jeschka danke ich für das Aufpolieren meiner ersten Konstruktionszeichnung (ohne das Herr Weis mich hochkant aus seiner Werkstatt geworfen hätte) – und natürlich für seine Hilfe in Computer-Angelegenheiten. Herr Jehle hat es ermöglicht, den edlen Inkubator um das Mikroskop zu konstruieren, und Frau Boczek und Frau Schönig-Erdinger waren eine große Hilfe bei administrativen Angelegenheiten.

Aus unserem Arbeitskreis gibt es einige Leute, mit denen ich näher zusammengearbeitet habe und denen ich im Folgenden danken möchte:

Alexandre und Jens haben mir eine solide Einführung in das Arbeiten in der Zellkultur, im Chemielabor, im Reinraum und am Delta-Vision gegeben. Wouter verdanke ich mein Wissen über Sputtern – und einige herausfordernde Badminton-Partien.

Daniel hat mich immer hilfsbereit und geduldig in chemischen Fragestellungen beraten, und Ada hatte stets ein offenes Ohr für biologische Probleme.

Thanks to Tamas for general support and teaching me the AFM cantilever calibration.

Theo danke ich für die REM-Messungen, lustige Pärchenabende und generell gute Unterhaltung(en). Von Simon habe ich die Feinheiten im Umgang mit SMS gelernt, und Babak hatte die großartige Idee mit dem Wiki (und der Festplatte..). Kai danke ich für die

Wertschätzung meiner LabView-Programme und erfrischend unkonventionelle Meinungen zu vielen Themen, Ilia für die Elastizitätsmessungen, Diskussionen über Bildverarbeitung und den Tip, nach Ecuador zu fliegen, und Aaron für die Organisation der Verpflegung während des Journal-Clubs und die Villa-Parties. Benedikt danke ich für seine Hilfe bei den Auswertungen der traction-force-Messungen.

Allen Mitgliedern des AK Spatz danke ich für eine inspirierende und abwechslungsreiche Arbeitsatmosphäre, extrem unterhaltsame Mittagessen und gemütliche Grillabende. Es hat Spaß gemacht, mit Euch zu arbeiten!

Der Universität Heidelberg danke ich für die netten Spanischkurse, das gute Essen und den Hochschulsport (besonders für die Beach-Plätze...). Und dafür, dass sie die Parkgebühren erst jetzt einführt.

Nach Leipzig bzw. Paris sende ich Grüße und Dank: Timo, Michel und dem Rest der Käs-Gang dafür, mein Interesse an Biophysik geweckt zu haben.

Ein weiterer Dank geht nach Übersee, von wo aus Timm mir ermöglicht hat, immer auf dem neuesten Wissenstand zu bleiben.

Die hier vorgestellten Experimente wurden erheblich erleichtert durch die Mithilfe einiger Studenten: Moritz Menacher, Steffen Wolff, Martin Pfannmöller, Stephanie Németh und Karina Drobbe haben durch ihre gewissenhafte Arbeit und ihren Einsatz erheblich zum Gelingen dieser Arbeit beigetragen.

Ein großer Dank geht auch an Christine, Jennifer und Mercedes, die durch Ihre Korrekturen dieser Arbeit den letzten Schliff gegeben haben.

Außerhalb des wissenschaftlichen Lebens danke ich meiner WG, die (in wechselnden Besetzungen) immer für Abwechslung gesorgt hat.

Meiner Familie danke ich ganz herzlich für den Rückhalt und die Unterstützung über all die Jahre. Ohne sie wäre ich nie so weit gekommen.

Zuletzt möchte ich der Person danken, die mir am nächsten steht und die gerade in den letzten Monaten am meisten unter dieser Doktorarbeit zu leiden hatte. Billy: Vielen Dank für das Verständnis und die Geduld, die Du aufgebracht hast. Und dafür, Dein Leben mit mir zu teilen!

Appendix

Abbreviations

AFM	atomic force microscopy
CFP	cyan fluorescent protein
DMEM	Dulbeccos Modified Eagle Medium
ECM	extracellular matrix
FA	focal adhesion
FWHM	full width at half maximum
FBS	fetal bovine serum
PAA	polyacrylamide
PDMS	polydimethylsiloxane
REF	rat embryonic fibroblast
YFP	yellow fluorescent protein

Supplementary Material

Videos corresponding to the image sequences presented in this thesis can be found at http://www.divshare.com/download/2214603-22f. They are not critical for the understanding of the work presented here, but illustrate the involved dynamics in a more vivid way than still images can.

Ich erkläre hiermit, dass ich die vorgelegte Dissertation selbst verfasst und mich keiner anderen als der von mir ausdrücklich bezeichneten Quellen und Hilfen bedient habe.

Heidelberg, den 1. Oktober 2007 .....

Patrick Heil